

Article

Parameter Matching and Optimization of a Hybrid Type DC SFCL Considering the Transient Characteristics of VSC-Based DC Systems

Siyuan Liang , Yuejin Tang, Li Ren *, Ying Xu, Jing Shi, Zheng Li and Xiangyu Tan

State Key Laboratory of Advanced Electromagnetic Engineering and Technology, School of Electrical and Electronic Engineering, Huazhong University of Science and Technology, Wuhan 430074, China; liangsiyuan@outlook.com (S.L.); tangyj@mail.hust.edu.cn (Y.T.); xuying@hust.edu.cn (Y.X.); shijing@mail.hust.edu.cn (J.S.); Hust_Liz@163.com (Z.L.); txym2018@hust.edu.cn (X.T.)

* Correspondence: renli@mail.hust.edu.cn; Tel.: +86-027-87544755

Received: 13 July 2019; Accepted: 8 September 2019; Published: 13 September 2019



Abstract: Voltage source converter-based (VSC-based) DC systems play an important role in connecting large-scale renewable energy and distributed energy, but they are vulnerable to DC short-circuit fault and lacks mature protection devices and appropriate protection strategies. Therefore, a hybrid type DC superconducting fault current limiter (H-SFCL) is proposed and the current limiting mechanism of the SFCL is analyzed. According to the requirements and strategies for protection, several different effective parameter matching and optimization methods of the H-SFCL are proposed by combining optimization algorithms and two short-circuit transient calculation models of VSC-based DC systems. The optimization methods proposed in this paper are compared and analyzed in terms of convergence, running time, calculation range and stability of optimization results, revealing their respective calculation characteristics. Finally, the effectiveness of parameter matching and optimization methods are well validated by comparison and analysis of simulation. The proposed methods can select a good parameter matching scheme of the H-SFCL to deal with different requirements.

Keywords: hybrid type DC SFCL (H-SFCL); DC circuit breaker (DCCB); voltage source converter (VSC); parameter matching; optimization

1. Introduction

Voltage source converter (VSC)-based DC transmission technology can realize active and reactive power controlling [1] and bus voltage supporting [2], which can restrain the fluctuation and randomness of renewable energy in a large range and has potential advantages in renewable energy paralleling in the power grid [3,4]. Meanwhile with a common DC voltage and easy parallel connections, VSC-based DC transmission technology is the most appropriate for multi-terminal DC systems (MTDC) [5]. As a promising research hotspot, several VSC-based demonstration projects have been built including the conventional two or three level converter and modular multi-level converter [6–10]. Nevertheless, the safe, reliable and continuous operation of VSC-based DC system is the premise of exerting its own advantages. Due to the low damping of the DC system, DC short-circuit fault with high current rising rate and fast fault propagation speed is a great threat to the VSC-based DC system [11], which requires the sensitivity of fault identification and the rapidity of protective action. According to [12,13], DC short-circuit current must be interrupted within 5 ms to ensure the safety of VSC components.

At present, there are three main methods to deal with DC short-circuit fault, including blocking trigger pulse of converter, opening all AC circuit breakers (ACCBs) on AC sides of the VSC system then opening DC circuit breakers (DCCBs) [13]. DC short-circuit current is difficult to be cleared because

of freewheel diodes [14]. Whereas, the first two methods must be adopted together in a VSC-based DC system in case of AC grids current feeding [15]. However, the first two methods have to force converter stations to shut down, which will have a negative impact on the continuous operation of a VSC-based DC system. DCCB can rapidly clear and isolate fault lines and maintain continuous operation of converter stations and other transmission lines, thereby preventing power transmission disruptions [16]. Therefore, DCCB is a better choice for the DC protection of VSC-based DC systems. With the capacity of power systems increasing, the economic cost and technical difficulty of DCCB become the main obstacles to the development of a VSC-based DC system [17].

The emergence of superconducting fault current limiter (SFCL) provides a good solution for solving DC short-circuit fault in a VSC-based DC system, which can improve the fault ride through capability and robustness of VSC-based DC systems [18,19] and assist DCCBs to interrupt [20–22]. According to current limiting components, DC SFCLs can be divided into a resistive type, an inductive type and a hybrid type [23]. Resistive type DC SFCL (R-SFCL) has been widely studied, including application in DC systems [24,25], economic and technical analysis [26] and engineering prototypes [27–29]. Some scholars have also carried out some studies on the performance of inductive type DC SFCL in VSC-based DC systems [30,31]. Based on the considerations of current limiting, recovery characteristics and energy dissipation, a comparative study of several types of DC SFCLs in VSC-based DC systems has been made in [32].

In addition, parameters' influence and matching of different current limiters (FCLs) in different DC systems have been studied extensively, which have provided a good theoretical basis for the applications of different FCLs in high voltage direct current (HVDC) systems, as shown in Table 1. The methods adopted in these studies are mainly enumeration, comparison, analytical formula and graphical method, which are very suitable for studying the variation rule of parameters' influence in FCLs.

Table 1. Studies on the parameters of fault current limiters in HVDC.

HVDC System	DC FCL/SFCL	Study on Parameters of SFCL/FCL			Method	Year
		Influence	Matching	Optimization		
VSC	Resistive Type [20]	Yes	No	No	Enumeration, Comparison	2015
VSC	Resistive, Inductive Type [18]	Yes	No	No	Enumeration, Comparison	2016
VSC	Hybrid Type [33]	Yes	Yes	No	Enumeration, Comparison	2017
MMC	Hybrid Type [13]	Yes	Yes	No	Analytical Formula, Graphical method	2017
Hybrid	Resistive Type [25]	Yes	No	No	Enumeration, Comparison	2018
MMC	Inductive type [34]	Yes	Yes	No	Analytical Formula, Comparison	2019
MMC	Resistive, Inductive, Hybrid Type [35]	Yes	Yes	No	Enumeration, Comparison	2019

However, it is obvious that there is still a lack of detailed studies on the combination of parameter matching and optimization methods of FCLs with multiple elements in DC systems, which are very important for the reasonable selection and design of FCLs' parameters to solve mutual influence and restriction among multiple parameters. Therefore, it is very necessary to carry out relevant research works before FCLs are installed in HVDC systems. At present, the optimization problems of FCLs mainly focus on AC systems, such as optimal power flow [36], optimal allocation [37–41], economic analysis [42] and protection coordination [43]. FCLs adopted in studies are mainly resistance type fault current limiters with simple structure. Therefore, these studies focus on issues at the level of AC system while ignoring FCL itself. In addition, short-circuit fault current in AC system is obtained by power flow calculation, which usually is a steady state calculation. However, transient calculation is more important in the short-circuit calculation of a DC system, which needs to be able to accurately calculate the transient characteristics of DC system within a short time range. When FCL has a complex

structure, its ontology performance should also be considered. Therefore, the optimization of FCLs in DC systems face new problems remaining to be solved.

In this paper, our study on a hybrid type SFCL (H-SFCL) is further developed based on previous studies of a small-scale prototype test and system simulation [44,45]. First, according to system simulation, the basic requirements and principles of the H-SFCL's parameter matching are put forward. Second, for radiation multi-terminal VSC-based DC systems, two short-circuit calculation models of VSC-based DC system with H-SFCLs are proposed which can accurately simulate the transient process of DC short-circuit fault. Third, based on the precision of simplified system models and the excellent ability of genetic algorithm (GA) and particle swarm optimization (PSO) in optimization, several parameter matching and optimization methods of the H-SFCL in system are effectively realized and compared. They consider the safety and stability of the superconducting part of the H-SFCL and present a good parameters selection and optimization effect, simultaneously satisfying the requirements of fault current limiting and the design parameters of the H-SFCL in a VSC-based DC system.

2. Hybrid Type DC Superconducting Current Limiter and DC Circuit Breaker

2.1. H-SFCL

Figure 1a signifies the basic topological structure of the H-SFCL [45], which is composed of two high power resistors R_1 and R_2 , a superconducting coil L_{SC} , a metal oxide arrester R_{MOA} , and a high-speed controlled switch S_1 . R_1 and R_2 are current limiting resistors. L_{SC} is smoothing inductance which is wound by high temperature superconducting (HTS) tape. R_{MOA} is applied to the transient overvoltage suppression of L_{SC} .

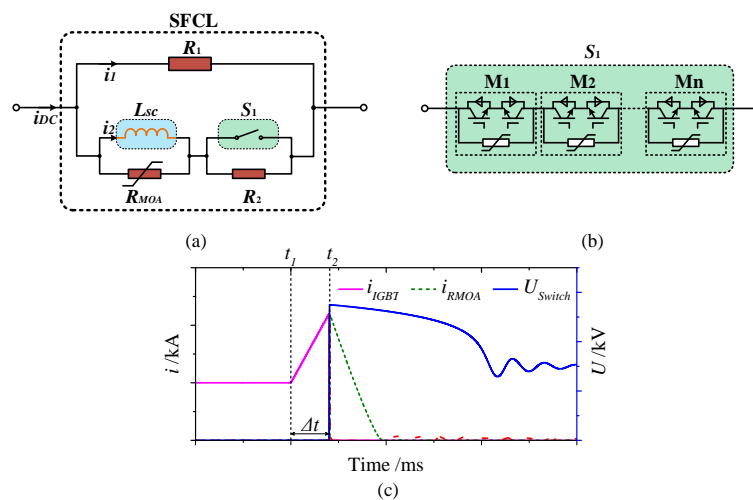


Figure 1. Topological structure. (a) Configuration of the hybrid type DC superconducting fault current limiter (H-SFCL); (b) high-speed controlled switch S_1 ; (c) the breaking characteristics of S_1 .

In this H-SFCL, high-speed controlled switch S_1 is a significant component for operational state transition, which must meet the rapidity and effectiveness of the H-SFCL. Due to the fast response characteristics of solid-state devices, a full solid-state DC fast switch can interrupt DC current within 100 μ s and has a great advantage in fast interrupting [46]. Therefore, it can be adopted as S_1 , whose basic structure is shown in Figure 1b. It can satisfy the breaking requirements of S_1 by series-parallel combination of basic unit. The breaking characteristics of S_1 are shown in Figure 1c, where t_1 is short-circuit fault time, t_2 is S_1 switch breaking time and Δt is breaking delay time including fault protection time t_{det} , protection coordination time t_{cod} and communication time t_{com} , which can be described as Equation (1) [47].

$$\Delta t = t_{det} + t_{cod} + t_{com} \quad (1)$$

2.1.1. Basic Principles of H-SFCL

In normal state, the switch S_1 is closed, as shown in Figure 2a. The DC current only flows through smoothing inductance L_{SC} , which operates at superconducting state without energy loss and has no effect on main circuit when DC system is in steady state. Low energy loss is very suitable for the long-term operation of equipment in series.

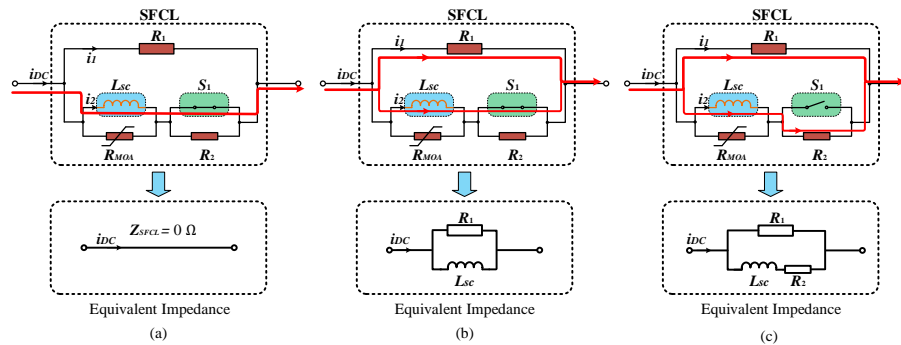


Figure 2. Principles of the H-SFCL. (a) Normal; (b) current limiting stage I; (c) current limiting stage II.

When short-circuit fault occurs, the H-SFCL can rapidly limit fault current without superconducting coil quenching, which has two current limiting stages [45]: current limiting stage I and current limiting stage II.

Current limiting stage I is shown in Figure 2b. When short-circuit fault occurs, the sudden change of current (di_2/dt) causes instantaneous impedance of the superconducting coil, forcing fault current to transfer to branch R_1 . R_1 is current limiting resistance and L_{SC} is current limiting inductance, which produce a transient current limiting impedance together to suppress initial impulse current. Meanwhile a shunt branch provided by R_1 greatly reduces the current flowing through L_{SC} , which weakens the impact of fault current on superconducting coil.

Current limiting stage II is shown in Figure 2c. After fault detection, S_1 is rapidly opened, and R_2 is put into the L_{SC} branch. It is worth noting that the quench of superconducting inductance coil is a very dangerous condition. R_2 can limit current i_2 to avoid exceeding the critical current of L_{SC} , which can protect L_{SC} from quenching. Meanwhile the H-SFCL gradually presents a steady equivalent current limiting impedance by R_1 in parallel with R_2 .

During operation, the equivalent impedance of the H-SFCL can be expressed by Equation (2), where t_1 is the time of fault occurrence and t_2 is the time of S_1 switching off. There is breaking delay time Δt between t_1 and t_2 , where $t_2 - t_1 = \Delta t$.

$$Z_{SFCL} = \begin{cases} 0 & (t < t_1) \\ \frac{L_{SC}}{i_2} \frac{di_2}{dt} \cdot R_1 / \left(\frac{L_{SC}}{i_2} \frac{di_2}{dt} + R_1 \right) & (t_1 \leq t < t_2) \\ \left(\frac{L_{SC}}{i_2} \frac{di_2}{dt} + R_2 \right) \cdot R_1 / \left(\frac{L_{SC}}{i_2} \frac{di_2}{dt} + R_2 + R_1 \right) & (t_2 \leq t) \end{cases} \quad (2)$$

2.1.2. Current Limiting Process Analysis in a VSC-Based DC System

Figure 3a is the diagram of DC short-circuit fault in a VSC-based DC system, which indicates that DC short-circuit fault can be divided into two types: ① pole-to-ground short-circuit fault; ② pole-to-pole short-circuit fault. Compared with pole-to-ground short-circuit fault, the equivalent voltage value of pole-to-pole short-circuit fault is U_{DC} which is twice the value of pole-to-ground, leading to a more serious short-circuit fault on the DC side. Therefore, considering the operation of the H-SFCL under the most serious DC fault, the analysis of the H-SFCL in pole-to-pole short-circuit fault is carried out.

Figure 3b shows the short-circuit current path of pole-to-pole DC fault in a pseudo bipolar VSC-based DC system, where two H-SFCLs are installed at the outlet of VSC converter station to suppress short-circuit current from DC-link capacitors discharging and AC grids feeding. As shown in

Figure 3b, due to the upper and lower symmetry of a VSC-based DC system, the general mathematical model of the H-SFCL can be established by analyzing unipolar line equivalent circuit.

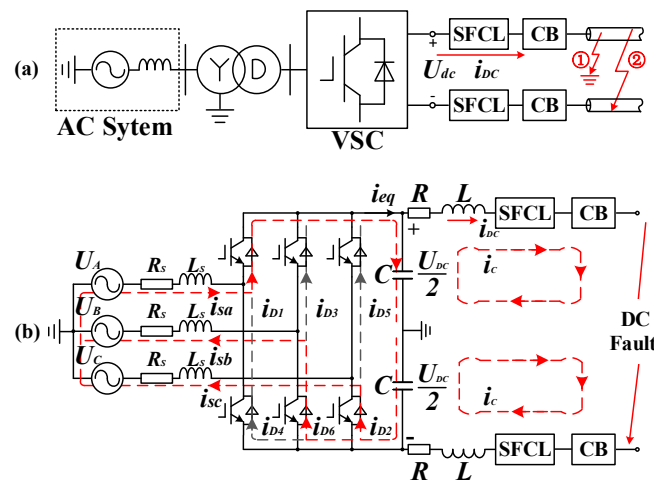


Figure 3. Schematic diagram of DC short-circuit fault. (a) DC short-circuit fault of VSC-based DC system. (b) Short-circuit current path of pole-to-pole DC fault in a pseudo bipolar VSC-based system.

The unipolar line equivalent circuit is shown in Figure 4, which is a third-order circuit. In this equivalent circuit, the AC system with rectifier is equivalent to a current source i_{eq} except for DC-link capacitor C . The influence of metal oxide arrester R_{MOA} and the energy releasing process of S_1 are both ignored. The DC system is a nonlinear dynamic system network in the process of short-circuit fault.

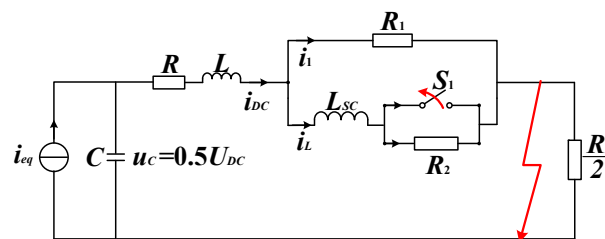


Figure 4. Unipolar line equivalent circuit.

Generally, in first and second order circuits, an analytical formula can be solved to clarify the mathematical relationship between circuit parameters [48]. However, when a circuit becomes third-order or even more complex, with the number of variables increasing, there are some difficulties in solving the analytical formula. The interaction between circuit parameters in dynamic networks can be clearly expressed by using a state variable matrix. In order to establish the mathematical equivalent model of the H-SFCL and express the transient effect of the H-SFCL accurately, the state variable analysis method is adopted, where t_1 is short-circuit fault time, t_2 is S_1 breaking time, R_L is the equivalent load on the DC side and u_C , i_{DC} and i_L are set as state variables.

The state variable matrix is:

$$X = [u_C \quad i_{DC} \quad i_L]^T. \tag{3}$$

The first-order derivative of the state variable matrix on t is:

$$\dot{X} = [\frac{du_C}{dt} \quad \frac{di_{DC}}{dt} \quad \frac{di_L}{dt}]^T. \tag{4}$$

When $t_1 \leq t < t_2$, S_1 is still in the closed state. The initial state of the state variables is:

$$\begin{cases} u_C(t_1^-) = u_C(t_1^+) = U_0 \\ i_{DC}(t_1^-) = i_{DC}(t_1^+) = i_L(t_1^-) = i_L(t_1^+) = I_0 \end{cases} \tag{5}$$

where $U_0 = 0.5U_{DC}$, $I_0 = (0.5U_{DC})/(0.5R_L)$.

The third-order state equation is established as follows:

$$\dot{X} = A_1X + BF(t). \tag{6}$$

When $t_2 \leq t$, S_1 is opened. The initial state of the state variables is:

$$u_C(t_2^-) = u_C(t_2^+), i_{DC}(t_2^-) = i_{DC}(t_2^+), i_L(t_2^-) = i_L(t_2^+). \tag{7}$$

The third-order state equation is established as follows:

$$\dot{X} = A_2X + BF(t), \tag{8}$$

where

$$A_1 = \begin{bmatrix} 0 & -1/C & 0 \\ 1/L & -(R_1 + R)/L & R_1/L \\ 0 & R_1/L_{SC} & -R_1/L_{SC} \end{bmatrix}, A_2 = \begin{bmatrix} 0 & -1/C & 0 \\ 1/L & -(R_1 + R)/L & R_1/L \\ 0 & R_1/L_{SC} & -(R_1 + R_2)/L_{SC} \end{bmatrix},$$

$$B = \begin{bmatrix} -1/C & 0 & 0 \\ 0 & 0 & 0 \\ 0 & 0 & 0 \end{bmatrix}, F(t) = [i_{eq}(t) \quad 0 \quad 0]^T.$$

2.2. DC Circuit Breaker

A DC circuit breaker is a critical protection device for a DC system, which bears the function of interrupting DC fault current and isolating a fault. At present, there are two typical demonstration projects of high voltage DCCBs in the world, hybrid DCCB (H-DCCB) and coupling mechanical DC circuit breaker (CM-DCCB), respectively shown in Figure 5a,b.

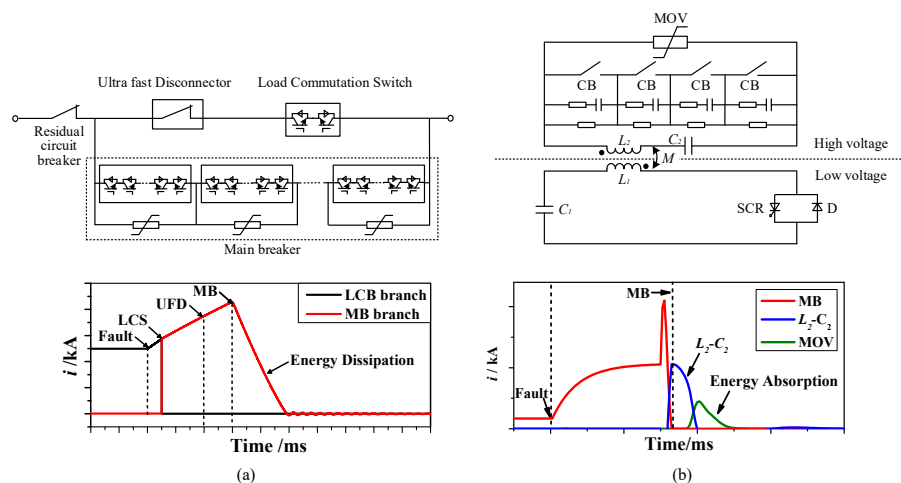


Figure 5. Two typical high voltage DC circuit breakers (DCCBs): (a) hybrid DCCB (H-DCCB); (b) coupling mechanical DCCB (CM-DCCB).

H-DCCB is designed by Asea Brown Boveri Ltd (ABB), which is composed of an ultra fast disconnector (UFD), a load commutation switch (LCS), a main breaker (MB) and a residual circuit breaker (RCB). During normal operation, current only flows through the UFD and LCS, the current in the MB is 0 A. With a short-circuit fault occurring, the LCS is blocked to transfer fault current to the MB branch. After the UFD is in an open state, the MB breaks fault current finally. According to [49], the 80 kV module of H-DCCB was tested, which had 2 kA rated current and could break 9 kA fault current. The delay time of the LCS opening was 250 μ s. The delay time of the UFD opening was 2 ms.

A CM-DCCB was designed and installed in the Nan'ao three-terminal VSC-HVDC system of China Southern Power Grid in 2017, which can cut off 9 kA within 5 ms [50]. The CM-DCCB is divided into a high voltage side and a low voltage side which are isolated by a coupling reactor. The high voltage side is composed of a main mechanical breaker (MB), resonance branch of L_2 and C_2 (L_2 - C_2 branch) and metal oxide varistor branch (MOV branch). The low voltage side consists of charging capacitor C_1 , primary side of coupling reactor L_1 and silicon controlled rectifier (SCR). The L_2 - C_2 branch generates an artificial zero crossing point in the MB branch to make the MB cut off. Mechanical contact separation requires about 3 ms [51].

2.3. Action Sequence of H-SFCL and DCCB

The appropriate coordination control between the H-SFCL and the DCCB can fully exert the current limiting function of the H-SFCL and significantly improve breaking capacity of the DCCB for protecting a VSC-based DC system from short-circuit fault.

2.3.1. Action Sequence of H-SFCL and H-DCCB

The corresponding action sequence of the H-SFCL and the H-DCCB is shown in Figure 6. When short-circuit fault occurs, the specific procedures are as follows.

t_1 - t_2 : Before S_1 opening, the H-SFCL is in current limiting stage I which produces a transient current limiting impedance for initial impulse current. The delay time of S_1 should be within 2 ms consisting of 1 ms fault detection time [52], 0.5 ms communication delay [16] and hundreds of microseconds action delay [46].

t_1 - t_5 : The H-SFCL is in current limiting stage II, which produces a steady current limiting impedance, limiting continuous fault current during the whole breaking process of the H-DCCB. Because the LCS and MB are both full solid-state switches, their delay time is very short, within several hundred microseconds. An UFD is mechanical switch with an ability to break circuit fast at zero current state within 2 ms. Residual energy in the system is absorbed by the MOV within a few milliseconds. However, delay time Δt_{2-3} should be controlled within a range to ensure that it meets the protection requirements of a VSC-based DC system in engineering application.

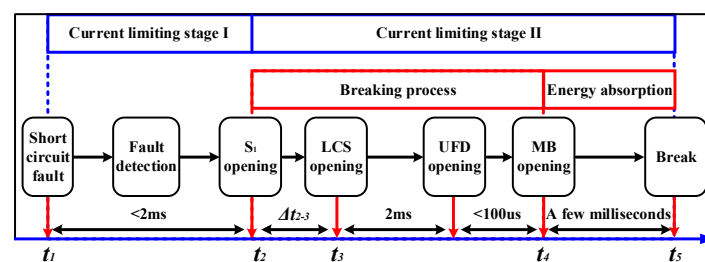


Figure 6. Action sequence of H-SFCL and H-DCCB.

2.3.2. Action Sequence of H-SFCL and CM-DCCB

The corresponding action sequence of H-SFCL and CM-DCCB is shown in Figure 7. When short-circuit fault occurs, the specific procedures are as follows.

t_1 - t_2 : This process is the same as the action sequence of H-SFCL and CM-DCCB, which is the inherent delay of H-SFCL.

t_2 - t_5 : H-SFCL is in current limiting stage II which produces a steady current limiting impedance, limiting continuous fault current during the whole breaking process of a CM-DCCB. The precharged capacitor C_1 discharges through SCR and L_1 , transferring energy to L_2 of the high voltage side at t_2 . L_2 - C_2 resonant circuit generates zero crossing point by the superposition of oscillating current and DC fault current on the MB. Meanwhile mechanical contact of the MB completes breaking at t_4 within about 3.2 ms. After a few milliseconds, residual energy is absorbed by the MOV to complete interrupting fault current at t_5 .

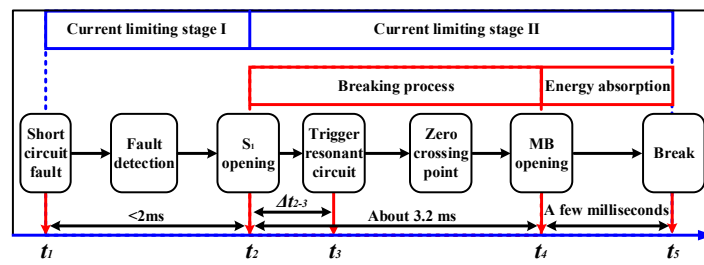


Figure 7. Action Sequence of H-SFCL and CM-DCCB.

3. Study on the Influence of H-SFCL Parameters

The H-SFCL has three main current limiting elements, R_1 , L_{SC} and R_2 . Their parameters directly affect current limiting of a VSC-based DC system. In addition, the parameter matching among components in the H-SFCL also affects their performance. Therefore, it is necessary to study the influence of H-SFCL parameters on itself and the VSC-based DC system.

3.1. VSC-Based System Simulation Model

As shown in Figure 8, a three-terminal VSC-based DC system model was established. The main purpose was to verify parameter effects of the H-SFCL on a VSC-based DC system including a converter station, H-SFCLs and DCCBs. The VSC-based DC system model was a traditional two-level structure whose rated capacity, rated voltage and rated current were respectively 100/50/150 MVA, ± 100 kV and 0.5/0.2/0.7 kA. The main system parameters are listed in Table 2.

The outlet of VSC1 station was an application scenario for short-circuit fault simulation, where two H-SFCLs were in series with DCCBs installed on positive and negative pole lines. Pole-to-pole short-circuit fault occurred between points a and b, which was the most serious DC short-circuit fault for VSC1 station. When bridge arm current I_p is greater than the operating current limit of insulated gate bipolar transistor (IGBT) and diode, converter stations are generally blocked.

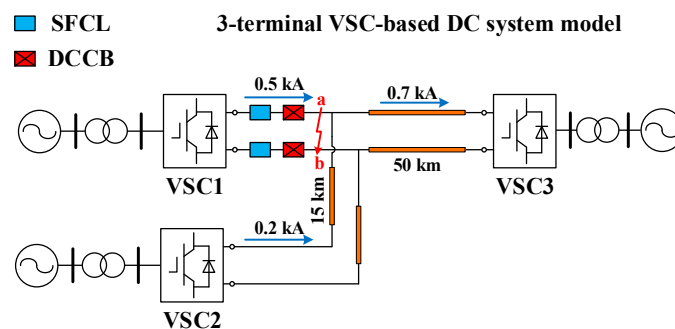


Figure 8. The diagram of three-terminal detailed VSC-based DC system simulation model.

Table 2. Main system parameters.

Parameters	Value	Parameters	Value
The type of converter station	Two-level	DC-link capacity, C (mF)	0.5
Rated capacity (MVA)	100/50/150	Resistance, R (Ω)	0.08
AC voltage (kV)	110	Smoothing inductance, L (mH)	20
Frequency, f (Hz)	50	Resistance per unit length of cable, Ω (km)	0.0139
DC voltage, U_{DC} (kV)	± 100	Inductance per unit length of cable, H (km)	0.159×10^{-3}
Rated DC current, I_{DC} (A)	500/200/700	Capacitance per unit length of cable, F (km)	12.74×10^{-9}
Current limit of IGBT and diode (kA)	2	Prospective maximum fault current (kA)	16.4

3.2. Simulation

Multivariable simulation cannot make clear the specific effect of each parameter in the H-SFCL. Therefore, changing single variable was adopted to clarify the influence of three parameters on the VSC-based DC system and the intrinsic performance of the H-SFCL. The simulation results covered nine aspects, such as DC-side voltage U_{DC} , DC line current I_{DC} , the current of freewheel diode I_{D1} , the current of the superconducting coil I_L , the overvoltage U_L of the superconducting coil, the magnetic energy E of the superconducting coil, current limiting impedance Z_{SFCL} , the overvoltage U_{S1} and the current I_{S1} of S_1 in the H-SFCL. t_1 is the time of fault occurrence. t_2 is the time of S_1 interruption in H-SFCL.

3.2.1. The Effect of R_1

In this set of simulations, L_{SC} and R_2 remained unchanged, and were set to 60 mH and 20 Ω , respectively. R_1 changed from 4 Ω to 16 Ω . The corresponding simulation results of nine characteristics are shown in Figure 9. On the premise of keeping R_2 and L_{SC} unchanged, increasing R_1 could bring significant effects on the VSC-based DC system and the H-SFCL.

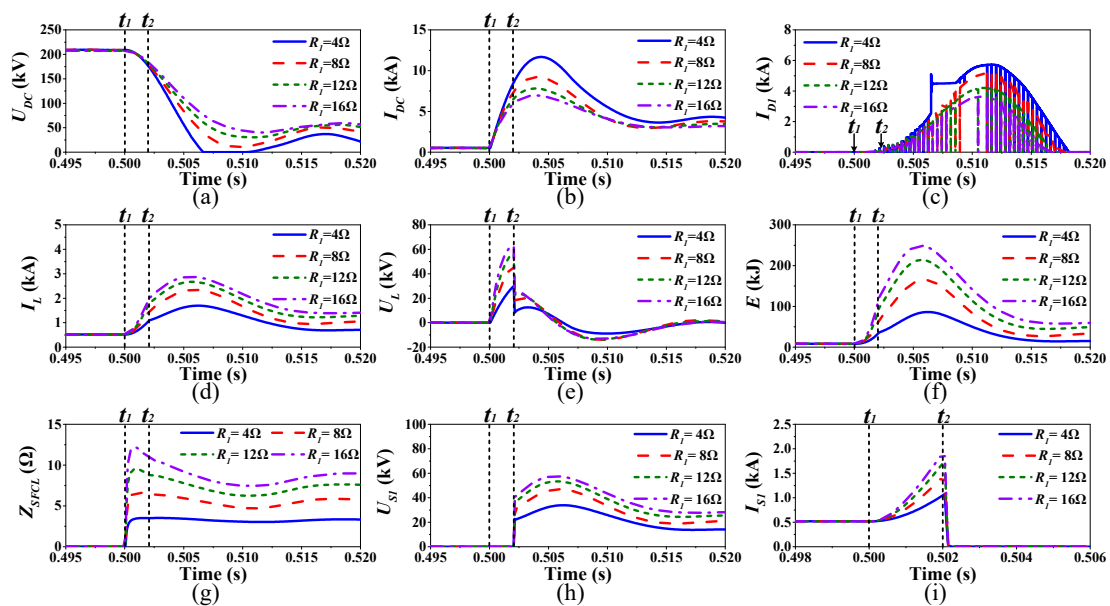


Figure 9. Comparison of the effects of different R_1 values. (a) DC-side voltage; (b) DC line current; (c) the current of freewheel diode; (d) the current of superconducting coil; (e) the overvoltage of superconducting coil; (f) the magnetic energy of superconducting coil; (g) current limiting impedance; (h) the overvoltage of S_1 ; (i) the current of S_1 .

Figure 9a–c indicates that increasing R_1 could obviously contribute to compensate DC voltage sag, while suppressing DC line current and the current of freewheel diode in the VSC-based DC system. The main reason was the equivalent current limiting impedance of the H-SFCL enhanced by increasing R_1 , as shown in Figure 9g. There is no doubt that increasing R_1 can reduce the effects of DC short-circuit fault and improve the robustness of the VSC-based DC system. Therefore, R_1 plays an important role in the H-SFCL to mainly bear the protection function at the system level.

On the contrary, increasing R_1 generated obvious negative effects on superconducting coil and S_1 . Figure 9d–f shows that increasing R_1 could easily cause a larger overcurrent, higher overvoltage and greater fluctuation of magnetic energy in the superconducting coil. Meanwhile, with R_1 increased, the overvoltage and current of high-speed controlled switch S_1 in the H-SFCL increase, which signified more severe operating conditions and higher economic cost of S_1 , as shown in Figure 9h,i.

3.2.2. The Effect of L_{SC}

In this set of simulations, R_1 and R_2 remained unchanged, and were set to 16Ω and 20Ω , respectively. L_{SC} changed from 80 mH to 140 mH. The corresponding simulation results of nine characteristics are shown in Figure 10.

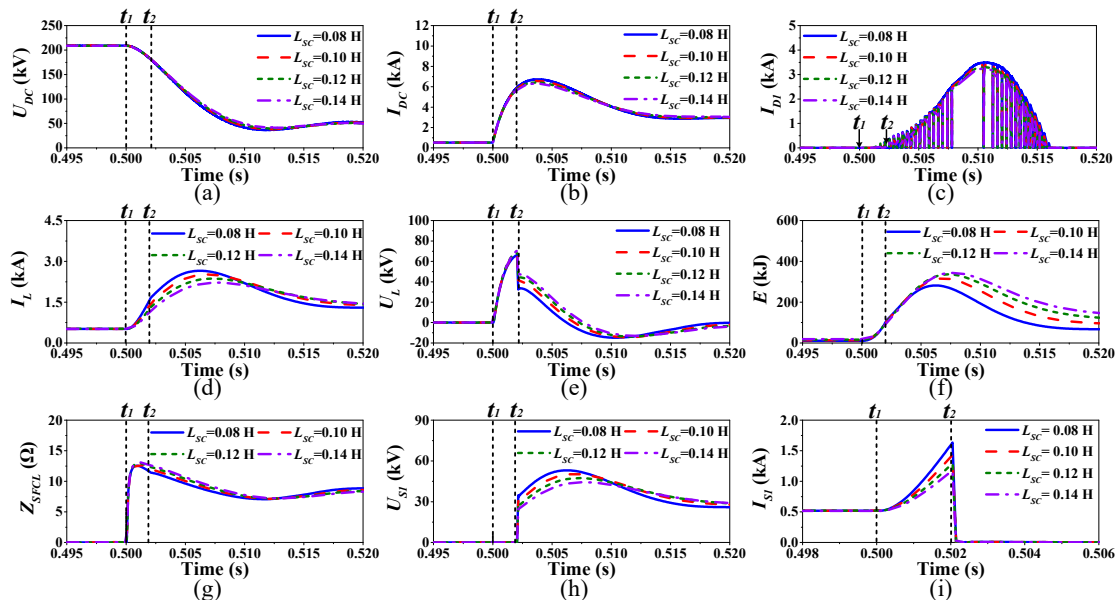


Figure 10. Comparison of the effects of different L_{SC} : (a) DC-side voltage; (b) DC line current; (c) the current of freewheel diode; (d) the current of superconducting coil; (e) the overvoltage of superconducting coil; (f) the magnetic energy of superconducting coil; (g) current limiting impedance; (h) the overvoltage of S_1 ; (i) the current of S_1 .

According to Figure 10g, increasing L_{SC} had a slight improvement of equivalent current limiting impedance in the H-SFCL. However, the limited change was not enough to significantly improve the performance of the VSC-based DC system under DC short-circuit fault, as shown in Figure 10a–c. Therefore, it indicated that L_{SC} is not the decisive parameter of current limiting effect for the VSC-based DC system.

However, Figure 10d–f reflects that increasing L_{SC} is a double-edged sword for the stable operation of the superconducting coil. On the one hand, during current limiting process, increasing L_{SC} could significantly reduce overcurrent in the superconducting coil, as shown in Figure 10d. On the other hand, it could cause higher overvoltage and greater fluctuation of magnetic energy in the superconducting coil, as shown in Figure 10e,f.

Figure 10h,i indicates that increasing L_{SC} provides a positive effect on high-speed controlled switch S_1 . With L_{SC} increased, the overvoltage and current of S_1 in the H-SFCL decrease, which contribute to reduce operating conditions and economic costs of S_1 .

3.2.3. The Effect of R_2

In this set of simulations, R_1 and L_{SC} remained unchanged, and were set to 16Ω and 140 mH, respectively. R_2 changed from 30Ω to 60Ω . The corresponding simulation results of nine characteristics are shown in Figure 11.

Figure 11g clearly reflects that increasing R_2 could enhance the steady current limiting impedance of H-SFCL after t_2 , while the transient current limiting impedance of H-SFCL had little improvement from t_1 to t_2 . Hence, in Figure 11a–c, it is not difficult to find that increasing R_2 only had a slight positive effect on DC-side voltage sag compensation and the current suppression of the DC line and anti-parallel freewheel diode in the VSC-based DC system. It suggests that R_2 is also not the decisive parameter of current limiting.

According to Figure 11d–f, the selection of R_2 is crucial to protecting the superconducting coil. Increasing R_2 has a positive effect on DC-side voltage sag compensation and the current suppression of DC line and anti-parallel freewheel diode, which is helpful to improve the safety and stability of the superconducting coil. However, increasing R_2 had some negative effects on high-speed controlled switch S_1 . Though the breaking current was not affected by increasing R_2 in Figure 11i, S_1 could withstand higher voltage stress in H-SFCL with R_2 increased, as shown in Figure 11g.

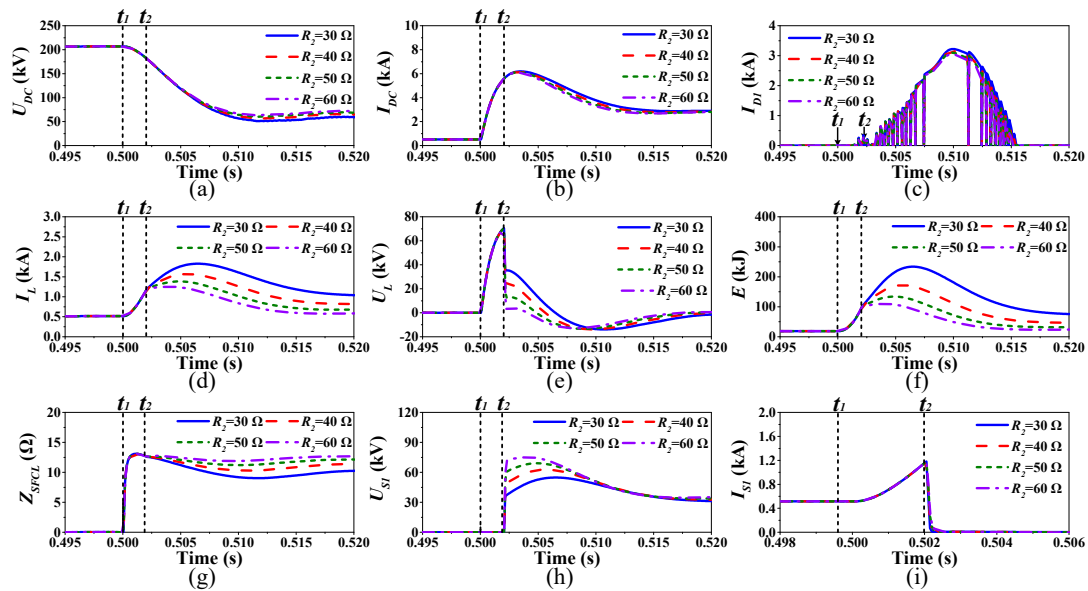


Figure 11. Comparison of the effects of different R_2 : (a) DC-side voltage; (b) DC line current; (c) the current of freewheel diode; (d) the current of superconducting coil; (e) the overvoltage of superconducting coil; (f) the magnetic energy of superconducting coil; (g) current limiting impedance; (h) the overvoltage of S_1 ; (i) the current of S_1 .

3.3. Summary

Through the above analysis, the effects of main parameters R_1 , R_2 and L_{SC} on the operational parameters of the H-SFCL and the VSC-based DC system were obtained, which are summarized in Table 3. It is worth noting that there are some contradictions in the effects of different parameters on specific functions in the H-SFCL. How to match various variables to maximize the target performance and achieve the compatibility of different functions in the H-SFCL is a difficult problem to be solved urgently. Therefore a parameter matching and optimization method is necessary to be developed to deal with the multi-parameter problems of a fault current limiter in a VSC-based DC system.

Table 3. The influence of main parameters of H-SFCL.

Affected Indicators		Main Influence Factors		
		$R_1 \uparrow$	$L_{SC} \uparrow$	$R_2 \uparrow$
VSC-based DC system	U_{DC}	+	/	/
	I_{DC}	-	/	/
	I_{D1}	-	/	/
H-SFCL	I_L	+	-	-
	U_L	+	+	-
	E	+	+	-
	Z_{SFCL}	+	/	+
	U_{S1}	+	-	+
	I_{S1}	+	-	/

“+”: increase; “-”: decrease; “/”: No significant effect.

4. Parameter Matching and Optimization Methods of H-SFCL in VSC-Based DC System

4.1. The Basic Requirements of Parameter Matching and Optimization in H-SFCL

When a H-SFCL is designed and applied in a VSC-based DC system, how to match and optimize the main parameters of H-SFCL should be considered comprehensively. There are three main aspects, namely the VSC-based DC system, the H-SFCL and the DCCB, shown in Figure 12.

First, at the system level, the H-SFCL should compensate DC-side voltage sag and limit DC line current. In addition, the H-SFCL should suppress the overcurrent of anti-parallel freewheel diode to weaken the impact of fault current on converter, ensuring overcurrent below the rated value of anti-parallel freewheel diode before DCCB breaking.

Second, at the H-SFCL level, on the premise of realizing target current limiting impedance, the parameters of main components in the H-SFCL should be selected reasonably by parameter matching and optimization to lower the operational conditions of the superconducting coil and S_1 , protecting them from the effect of fault current shock.

Third, at the DCCB level, the appropriate parameters of the H-SFCL should be selected to reduce the breaking current, voltage stress and energy absorption of the DCCB, which can improve the breaking capacity of the DCCB. In general, if the parameters of the H-SFCL can meet the current limiting requirements of system, the H-SFCL also meet the technical requirements of the DCCB.

Therefore, the selection of a parameter matching and optimization method should meet the following conditions:

- Multiple transient characteristic parameters of VSC-based DC system can be accurately calculated and acquired;
- More than three characteristic variables can be screened and optimized at the same time;
- Under multiple constraints, the optimal parameters can be searched and obtained according to the optimization objectives.

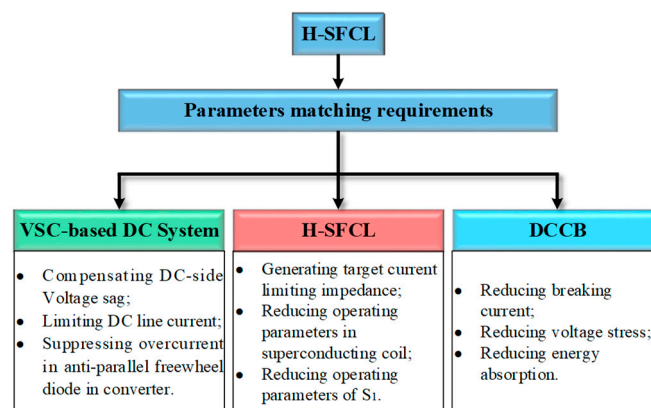


Figure 12. The basic requirements of parameter matching and optimization in H-SFCL.

4.2. The Implementation Methods of Parameter Matching and Optimization in the Transient Simulation of VSC-Based DC System Model

4.2.1. Short-Circuit Calculation Models

Before optimization, it is very important to accurately obtain the transient characteristic values of the VSC-based DC system. Therefore, it is necessary to establish an effective short-circuit calculation model. In the evolution process of a short-circuit fault, the VSC-based DC system is a typical AC/DC system which has a strong nonlinear dynamic network structure. Because the state variable matrix can correctly reflect the influence of multiple line variables on transient characteristics in any order circuit, even a complex system network, it is very applicable to calculate characteristic values in a system.

Two short-circuit calculation models based on state matrix are developed: (1) a simplified Simulink system model with a state matrix of the H-SFCL; (2) the state matrix model of equivalent capacitor discharging circuit. The first model is the hybrid computing model including Simulink model and state matrix codes. The second model is the equivalent computing model only having self-implemented state matrix codes.

(1) A Simplified Simulink Model with State Matrix (Hybrid Model)

The combination of a state matrix model of the SFCL and a Simulink model of a VSC system is the one of important parts in parameter matching and optimization. Figure 13a shows the equivalent short-circuit model of a VSC single-terminal system with two SFCLs, SFCL1 and SFCL2. The two SFCLs are both composed of state matrix and controlled current sources. The detailed model of SFCL1 in MATLAB/Simulink is shown in Figure 13b. In Figure 13b, controlled current sources 1 and 2 are respectively used to simulate two main branches of the SFCL, i_1 and i_L , changes of which can be equivalent to the working process of the SFCL in a VSC system. The parallel resistance of controlled current sources is required to ensure the model runs without reporting errors, and must be set large enough to avoid affecting calculation results. Gain1, Gain2 and Gain3 are used as input modules of variable assignment, and are convenient for an external program to identify and assign the parameters of the state matrix of SFCL.

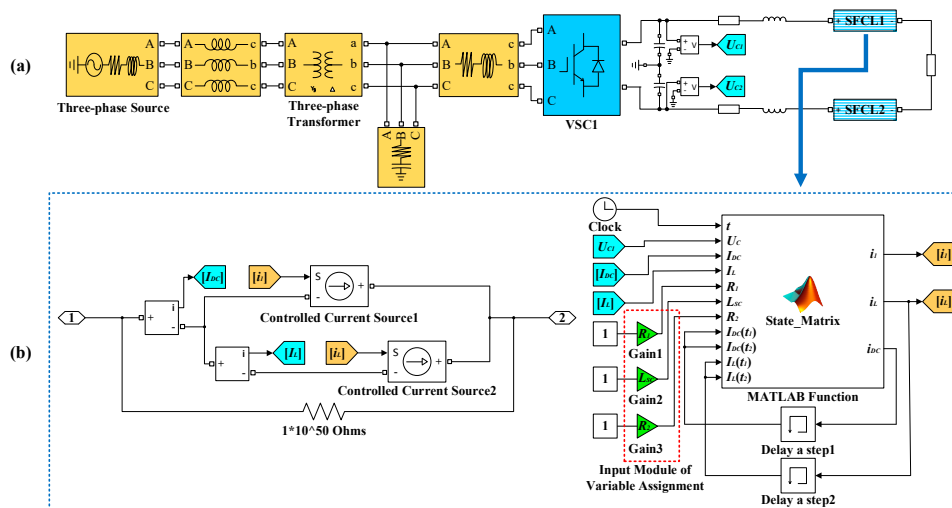


Figure 13. The model in MTALAB/Simulink. (a) The equivalent short-circuit model of a VSC single-terminal system. (b) The detailed model of SFCL1.

In order to improve solution speed of MATLAB/Simulink, a discrete simulation environment is adopted. When simulation step size T_S is set to a very small value, the Simulink model and state equations satisfy Equation (9):

$$\begin{cases} u_C(k_{n+1}) = u_C(k_n) + \frac{u_C(k_{n+1}) - u_C(k_n)}{k_{n+1} - k_n} T_S \\ i_{DC}(k_{n+1}) = i_{DC}(k_n) + \frac{i_{DC}(k_{n+1}) - i_{DC}(k_n)}{k_{n+1} - k_n} T_S \\ i_L(k_{n+1}) = i_L(k_n) + \frac{i_L(k_{n+1}) - i_L(k_n)}{k_{n+1} - k_n} T_S \end{cases} \quad (9)$$

where $k_{n+1} - k_n = T_S$. When T_S approaches 0, the following equation can be obtained:

$$\lim_{T_S \rightarrow 0} \frac{u_C(k_{n+1}) - u_C(k_n)}{k_{n+1} - k_n} = \frac{du_C}{dt}, \quad \lim_{T_S \rightarrow 0} \frac{i_{DC}(k_{n+1}) - i_{DC}(k_n)}{k_{n+1} - k_n} = \frac{di_{DC}}{dt}, \quad \lim_{T_S \rightarrow 0} \frac{i_L(k_{n+1}) - i_L(k_n)}{k_{n+1} - k_n} = \frac{di_L}{dt}. \quad (10)$$

Therefore, during current limiting process, according to Equations (9) and (10), the solution relationship of state matrix in the H-SFCL model can be approximately described as follows.

1) When $t_1 \leq k < t_2$,

$$X(k_{n+1}) = X(k_n) + [A_1X(k_n) + BF(k_n)]T_S. \quad (11)$$

2) When $t_2 \leq k$,

$$X(k_{n+1}) = X(k_n) + [A_2X(k_n) + BF(k_n)]T_S. \quad (12)$$

Through state matrix Equations (11) and (12),

$$i_1(k_{n+1}) = i_{DC}(k_{n+1}) - i_L(k_{n+1}). \quad (13)$$

(2) The State Matrix of Equivalent Capacitor Discharging Circuit (Single Model)

Compared with Figure 4, this method only considers the capacitor’s discharging process of a VSC-based DC system in short-circuit fault while ignoring the AC side current feeding. The capacitor discharging process is generally no more than 10 ms, which is exactly the key link of fault protection in a DC system [48]. Therefore, the SFCL mainly works during this 10 ms after DC fault occurrence. Equivalent capacitor discharging circuit is shown in Figure 14.

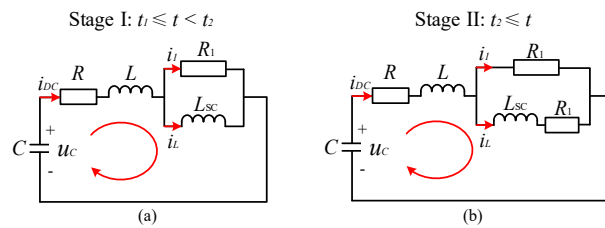


Figure 14. Capacitor discharging circuit: (a) $t_1 \leq t < t_2$, S_1 is in on state; (b) $t_2 \leq t$, S_1 is in off state.

Similar to the first model, discrete computation is adopted by programming in this model to solve transient characteristic quantities of system. n is set as the number variable of iterations. Fault occurs at t_1 . S_1 is off at t_2 . T_S is time step. According to Equations (3)–(8), in discrete calculation, the state matrix of equivalent capacitor discharging circuit can expressed by Equation (14).

$$\begin{cases} t(n) = nT_S \\ X(1) = [0.5U_0 \quad I_0 \quad I_0]^T \\ X(n+1) = X(n) + A_1X(n)T_S & 1 \leq n < (t_2 - t_1)/T_S \\ X(n+1) = X(n) + A_2X(n)T_S & (t_2 - t_1)/T_S \leq n \\ i_1(n) = i_{DC}(n) - i_L(n) \\ u_{DC}(n) = 2u_C \end{cases} \quad (14)$$

A set of parameters is assigned to R_1 , L_{SC} and R_2 to implement simulation comparison between two short-circuit calculation models, where $R_1 = 15 \Omega$, $L_{SC} = 100 \text{ mH}$, $R_2 = 80 \Omega$; corresponding simulation results shown in Figure 15. Computational characteristics of two short-circuit calculation models are summarized in Table 4.

Table 4. Comparison of short-circuit calculation models.

Model	Implementation Method	Precision	Effective Scope of Precision	Calculation Speed
Hybrid model	Simulink model + State Matrix Codes	High	The whole process	General
Single model	State Matrix Codes	Medium	Within 10 ms after fault	Fast

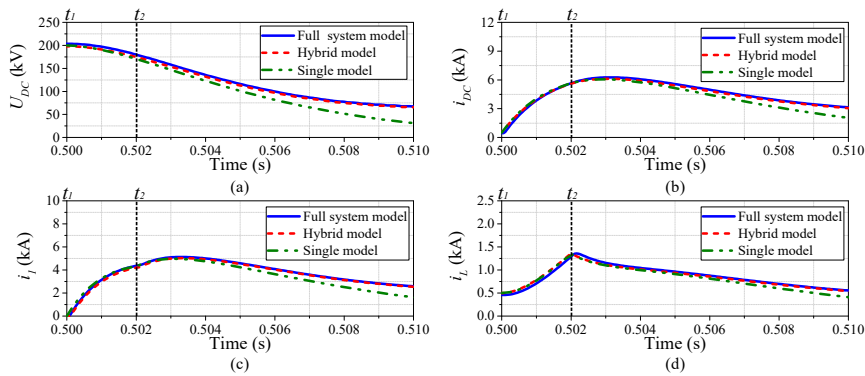


Figure 15. The simulation comparison: (a) the DC-side voltage, U_{DC} ; (b) the DC-line current, I_{DC} ; (c) the current of R_1 , i_1 ; (d) the current of L_{SC} , I_L .

4.2.2. Basic Implementation Workflows of Parameter Matching and Optimization Methods

R_1 , L_{SC} and R_2 are the main key components affecting current limiting performance of the SFCL, and are set as optimization variables. The method of parameter matching and optimization consists of three parts: optimization algorithm main program, objective function and constraints, and a short-circuit calculation model. Based on two short-circuit calculation models, there are two basic implementation workflows of parameter matching and optimization, as shown in Figure 16.

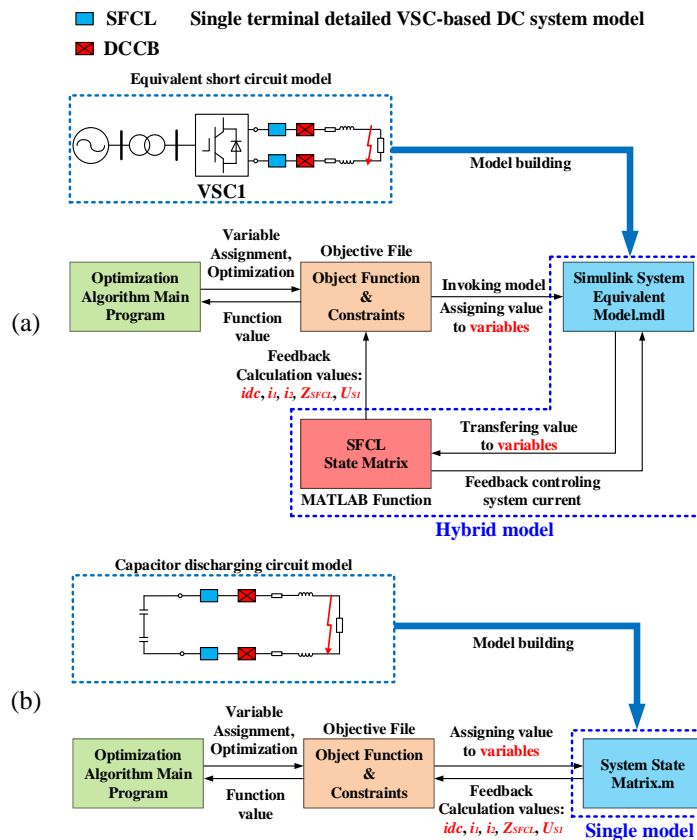


Figure 16. Basic implementation frameworks of parameter matching and optimization methods. (a) Basic frameworks based on hybrid model; (b) basic frameworks based on single model.

In Figure 16a, hybrid model consists of the Simulink system model and the state matrix of H-SFCL. MATLAB function is adopted to set up the state matrix of the H-SFCL which can simulate the SFCL in

the Simulink model and save calculation results for objective function reading. However, in Figure 16b, transient calculation and data storage are both completed by a single system state matrix model.

In the optimization process, the two implementation workflows are basically same. Optimization variables are firstly initialized through optimization algorithm main program, which are input into an objective function. The objective function assigns the value of variables to a short-circuit calculation model. Then, transient calculation is performed to obtain the characteristic quantities of the H-SFCL and system, which are fed back to the objective function for judgment and calculation. The results of the objective equation will return to the main program to determine whether the optimization is completed. If the stopping criteria is not met, the variables will be optimized in the next round.

4.3. Constraint Conditions and Fitness Function

In the whole current limiting process, first of all, the parameters of SFCL should meet the following constraints simultaneously.

- 1) The fault current limiting rate should satisfy the system requirement:

$$\frac{I_p - I_p'}{I_p} \times 100\% \geq K, \quad (15)$$

where I_p is the peak value of prospective short-circuit fault current, I_p' is the peak value of short-circuit fault current with SFCL and K is the minimum fault current limiting rate for the system requirements. Proper current limiting rate is helpful to restrain voltage sag and short-circuit current of the DC side and reduce the operating conditions of the DCCB.

- 2) The maximum current value flowing through L_{SC} should be lower than critical current to avoid L_{SC} quenching and ensure safe operation of L_{SC} . So:

$$I_{Lmax} \leq \alpha I_{rated} = I_c, \quad (16)$$

where I_{Lmax} is the maximum current value of L_{SC} , I_{rated} is the rated DC-line current of the VSC terminal, I_c is the critical current of L_{SC} and α is a coefficient greater than 1 which should be set as an appropriate value to provide a margin for safe operation of L_{SC} . Meanwhile current limiting in L_{SC} can also contribute to reduce the breaking current of S_1 .

- 3) The equivalent steady current limiting impedance of SFCL should exceed the minimum current limiting impedance required for the system, thereby:

$$Z_{steady} \geq Z_{required} \quad (17)$$

where $Z_{steady} = R_1 \times R_2 / (R_1 + R_2)$ and $Z_{required}$ is the minimum current limiting resistance required for the system.

- 4) During the current limiting process, the overvoltage of S_1 should be lower than the rated voltage of S_1 , so:

$$U_{over} \leq U_{rated}, \quad (18)$$

where $U_{over} \approx R_2 \times I_{Lmax}$ and U_{rated} is the rated voltage of S_1 . The number of IGBTs depends on the overvoltage of S_1 during S_1 interrupting current i_L .

On the premise of meeting above constraints, the objective function is designed to select optimal parameters to minimize the maximum transient magnetic energy of the superconducting coil, which is described as follows:

$$f(R_1, L_{SC}, R_2) = E_{max} \quad (19)$$

where $E_{max} = L_{SC} \times I_{Lmax}^2/2$. The superconducting coil is the core component of the H-SFCL, whose safety and stability of operation have great influence on the overall performance of the H-SFCL. AC loss is an important index of superconducting devices, which is usually caused by external time-varying field and transport current. It exists in coated superconductors and consists of hysteresis losses and eddy-current loss [53]. AC loss can cause joule heat, which has a negative effect on the steady operation of superconducting devices. Based on the results of [45], in the current limiting process, decreasing magnetic energy can help to reduce AC loss generated from current fluctuations in the superconducting coil. In addition, according to [54], the total length of superconducting tape is proportional to magnetic energy in different types of superconducting inductive coils. Optimizing magnetic energy can effectively reduce the amount of superconducting tape used in the coil and improve the economy of H-SFCL in engineering application. Therefore, it is necessary to optimize the maximum magnetic energy of superconducting coils.

4.4. The Workflows of Optimization Algorithms

4.4.1. The Optimization Workflows Based on GA

GA is a classical evolutionary algorithm, which is based on survival of the fittest and searches for the optimal solution in the problem space using selection, crossover and mutation operations [55]. It can solve complicated optimization problems from a variety of sources with outstanding advantages of simplicity, good robustness, implicit parallelism and global searching [56–60]. Therefore, based on GA, two optimization workflows of a H-SFCL applied in a VSC system are proposed as follows.

(1) GA Workflow 1

Figure 17 presents an optimization workflow based on GA, where R_1 , L_{SC} and R_2 in the SFCL are taken as the optimization variables. The selection of the variables plays an important role in the stability and reliability of a VSC-based DC system. Therefore, appropriate optimization conditions need to be set to ensure that the H-SFCL meets the requirements of the system. According to the constraint conditions proposed, R_1 , L_{SC} and R_2 can be selected and optimized to obtain optimal parameters, minimizing the maximum transient magnetic energy of the superconducting coil. In the process of iteration, the initial solution populations are randomly generated. If parameters selected do not satisfy optimization conditions, high fitness individuals will be selected to evolve a better individual population through crossover and mutation. The evolution process continues until stop conditions are satisfied. The purpose of a penalty function is to transform constrained optimization into unconstrained optimization. The GA workflow is simple and easy to implement, and can be adopted in the optimization of different current limiting devices without considering the detailed analysis of the relationship among variables.

(2) GA Workflow 2

In the Section 3.2, simulation results indicated that R_1 is the decisive parameter of the H-SFCL in current limiting process at a system level. Increasing R_1 can enhance current limiting effect, while the effects of R_2 and L_{SC} are not obvious on the system. In addition, reducing R_1 can effectively lower operating conditions of the superconducting coil and S_1 . Therefore, based on these characteristics of the H-SFCL, another optimization, Workflow 2, is proposed and shown in Figure 18.

Reaching the current limiting rate of the system is the primary requirement of R_1 selection. The initial values of L_{SC} and R_2 are set and remain unchanged. Then, the minimum value of R_1 is selected based on meeting the requirement of current limiting rate, which can effectively meet the current limiting requirements of the system and minimizes the influence of R_1 on the superconducting coil and S_1 . Meanwhile the selection range of R_2 can be determined by R_1 in advance. Thus, the data preprocessing can reduce the number of optimal variables and solution space by taking advantage of the characteristics of the H-SFCL in Table 3. Then, L_{SC} and R_2 are optimized as variables in GA. In the optimal solution set of minimum E_{MAX} , the parameter combination with the lowest overvoltage is

obtained by sorting and filtering optimization results. This link can avoid the instability of output results caused by the existence of multiple solutions in an optimal function value. Meanwhile this link can ensure that the parameter combination obtained in each optimization has the best performance in the optimal solution set.

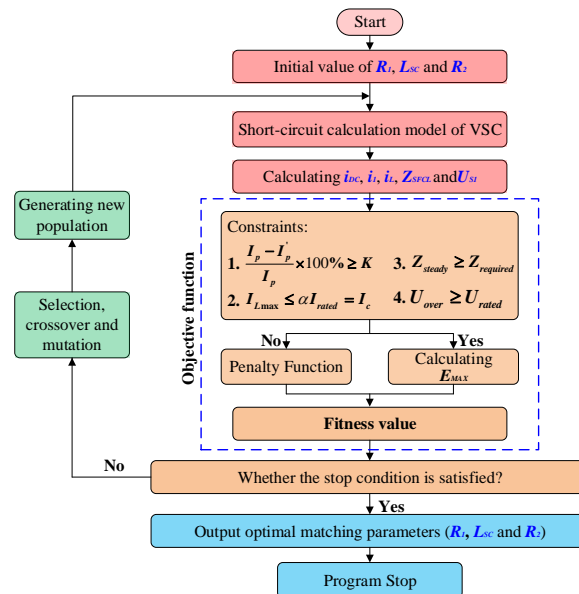


Figure 17. The optimization Workflow 1 based on genetic algorithm (GA).

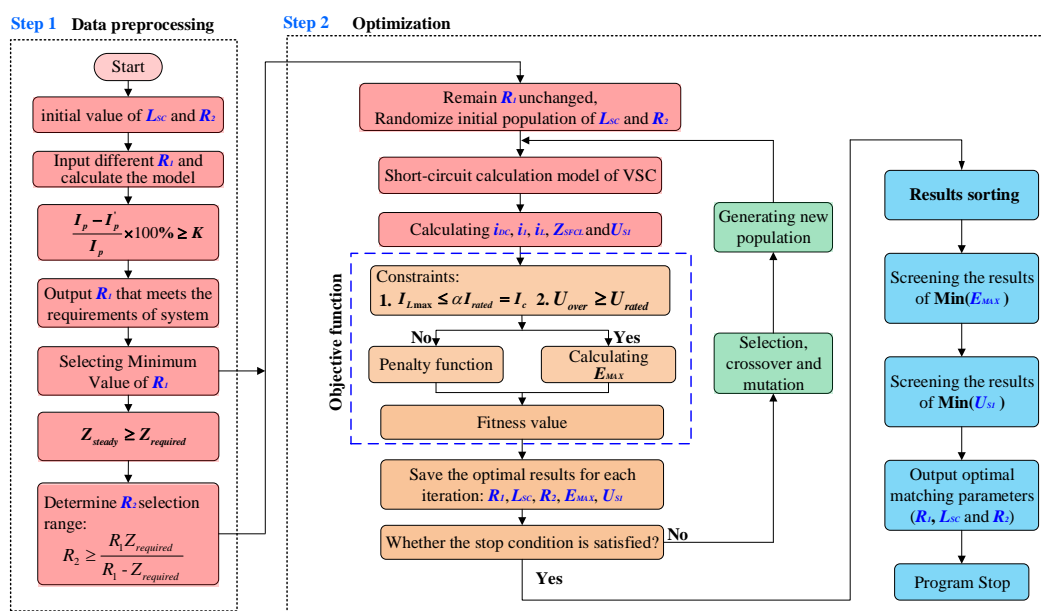


Figure 18. The optimization Workflow 2 based on GA.

4.4.2. The Optimization Workflow Based on PSO

PSO is an evolutionary algorithm proposed in 1995 [61], whose concept was inspired by studying on the rules of bird group behaviors during predation. Each particle in particle swarm represents a possible solution of the problem, which flies through solution space with random velocity and updates position to search for an optimal solution. PSO has the advantages of a simple algorithm, easy implementation and fast convergence speed in the aspects of spatial function optimization and dynamic target optimization, so it is very suitable for engineering applications [62–64].

The particle has two properties: velocity and position. Velocity represents the speed of movement and position represents the direction of movement. Generally, in the N -dimensional solution space, for m initial particles, the updates of their velocities and positions can be expressed by Equations (20) and (21) in the optimization process.

$$V_i = \omega V_i + c_1 r_1 (p_{best} - X_i) + c_2 r_2 (g_{best} - X_i), \tag{20}$$

$$X_i = X_i + V_i, \tag{21}$$

where X_i and V_i are respectively the position and velocity of each particle, p_{best} is the individual historical best position, g_{best} is the optimal position of the particle swarm, c_1 and c_2 are learning factors, r_1 and r_2 are random numbers between 0 and 1 and ω is inertia weight between 0.1 and 0.9. Based on PSO, two optimization workflows of the H-SFCL applied in a VSC system are proposed as follows.

(1) PSO Workflow 1

Figure 19 presents an optimization workflow based on PSO. R_1 , L_{SC} and R_2 in the SFCL are taken as the optimization variables, whose combinations are considered as particles flying in the search space. The current position of a particle is a candidate solution to the optimization problem. The flying process of particle is the process of a searching individual. The V_i and X_i of a particle can be dynamically adjusted by p_{best} and g_{best} . Through iteration, the velocity and position of particles are constantly updated, and the optimal solution satisfying termination conditions is obtained.

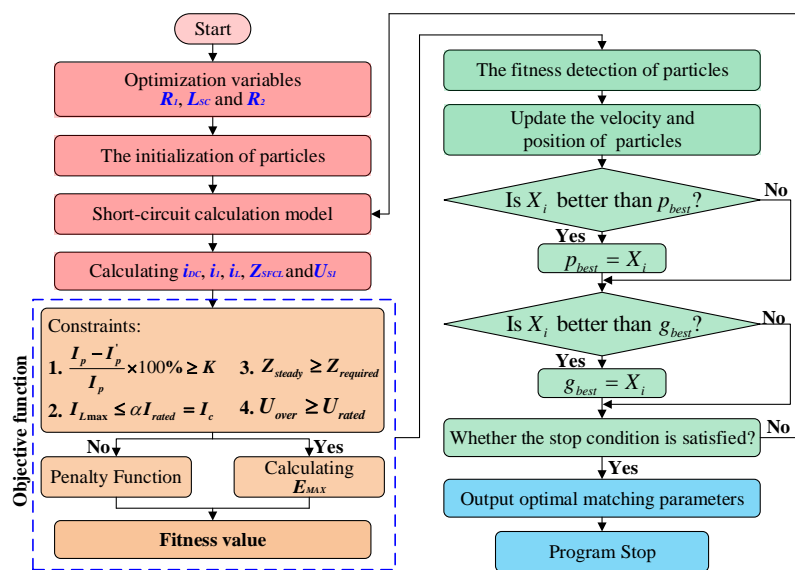


Figure 19. The optimization Workflow 1 based on particle swarm optimization (PSO).

(2) PSO Workflow 2

Figure 20 is an improvement based on PSO Workflow 1, which is similar to GA Workflow 2, adding data preprocessing and results sorting. The purpose of data preprocessing is to make optimization more targeted and directional. The purpose of results sorting is to avoid instability of optimization results and find the best combination of performance.

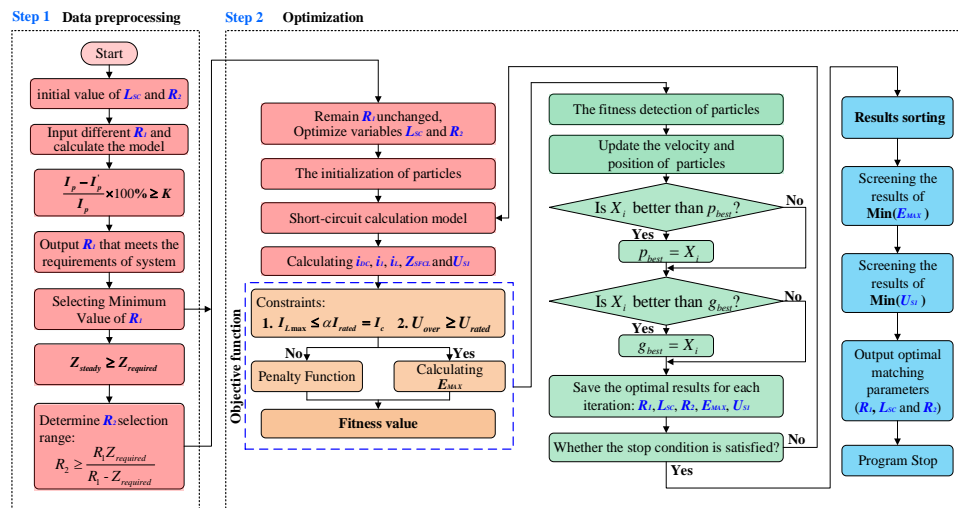


Figure 20. The optimization Workflow 2 based on PSO.

5. Case Study and Analysis

5.1. The Settings of Parameter Matching and Optimization

In parameter matching and optimization, taking the speed and accuracy of simulation into consideration, the step size of discrete simulation was 5×10^{-5} s. R_1, L_{SC}, R_2 were the main optimization variables. Because the parameters of components in the H-SFCL cannot be manufactured with precision to the last few decimal places, the data type of optimization variables was set as integer. The fault current that a DCCB can break is 9 kA, which is 54.9% of maximum short-circuit current (16.4 kA). Thus, fault current limiting rate should be no less than 50% to ensure that DCCB can break rapidly and reliably with the maximum short-circuit current of the system lower than 9 kA. The coefficient α was set as 3, so the peak value of the current in L_{SC} could be constrained within 1.5 kA. Meanwhile the minimum resistance required to limit the current was 8 Ω , and the rated voltage between the ends of S_1 was set not to exceed 80 kV. These multiple performance indices can be adjusted according to the system requirements.

Corresponding settings of GA Workflows 1 and 2, and PSO Workflows 1 and 2 are listed in Tables 5 and 6. In the data preprocessing of optimization Workflow 2, since current limiting rate was no less than 50%, the variation trend of current limiting rate with R_1 could be obtained by parameter scanning, shown in Figure 21. Therefore, the minimum value of R_1 satisfying 50% current limiting rate was 9 Ω . According to Equation (17), the selection range of R_2 could be determined; $R_2 \geq 72 \Omega$.

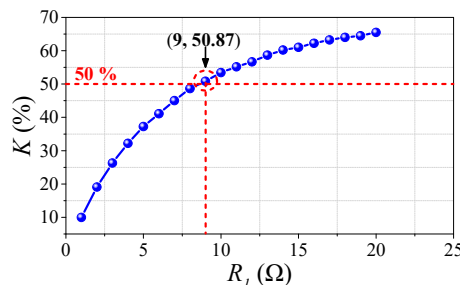


Figure 21. The variation trend of current limiting rate with R_1 .

Table 5. The main settings of GA Workflows 1 and 2.

		Workflow 1	Workflow 2
Time Step T_s		5×10^{-5} s	5×10^{-5} s
Optimization variables		R_1, L_{SC}, R_2	L_{SC}, R_2
Number of variables		3	2
Type of variables		Integer	Integer
Population size		40	40
Mutation rate		0.9	0.9
Crossover ratio		0.08	0.08
Generations		300	300
Stall generations		50	50
Function tolerance		1×10^{-6}	1×10^{-6}
Optimization variables range	R_1 (Ω)	5–50	9
	L_{SC} (mH)	10–200	(10–200)
	R_2 (Ω)	10–100	(72–100)
Constraint conditions	K	$\geq 50\%$	/
	α	≤ 3	≤ 3
	$R_{required}$	$\geq 8 \Omega$	/
	U_{rated}	≤ 80 kV	≤ 80 kV

Table 6. The main settings of PSO workflow 1,2.

		Workflow 1	Workflow 2
Time Step T_s		5×10^{-5} s	5×10^{-5} s
Optimization variables		R_1, L_{SC}, R_2	L_{SC}, R_2
Type of variables		Integer	Integer
Dimension, N		3	2
Number of particles		10	10
Maximum velocity of particles		20	20
learning factors, c_1, c_2		1, 2	1, 2
Initial inertia weight		0.9	0.9
Final inertia weight		0.4	0.4
Maximum iteration number		300	300
Minimum global error gradient		1×10^{-6}	1×10^{-6}
Iterations before error gradient criterion terminates run		50	50
The range of particles	R_1 (Ω)	5–50	9
	L_{SC} (mH)	10–200	10–200
	R_2 (Ω)	10–100	72–100
Constraint conditions	K	$\geq 50\%$	/
	α	≤ 3	≤ 3
	$R_{required}$	$\geq 8 \Omega$	/
	U_{rated}	≤ 80 kV	≤ 80 kV

5.2. The Results of Parameter Matching and Optimization

5.2.1. Global Optimal Solution

In order to verify the accuracy of parameter matching optimization methods, grid search (brute force approach) was adopted to search the global optimal solution. According to optimization Workflow 2 in GA and PSO, L_{SC} and R_2 had 5539 combinations in the integer space, as shown in Figure 22.

When $U_{rated} \leq 80$ kV and $\alpha \leq 3$, the feasible solutions were obtained according to the constraint conditions, as shown in Figure 23. In the feasible solutions, low U_{s1_max} was required while ensuring minimum value of E_{max} . Therefore, global optimal solution was $(R_1, L_{SC}, R_2) = (9, 111, 72)$ and $E_{max} = 61.65635419$.

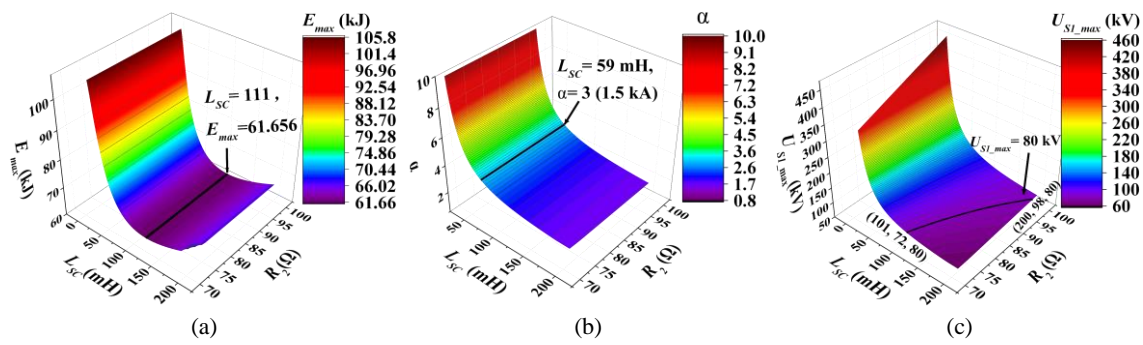


Figure 22. All calculation results in search space: (a) maximum transient magnetic energy; (b) ratio of designed critical current to rated current of superconducting coil; (c) maximum overvoltage of S_1 .

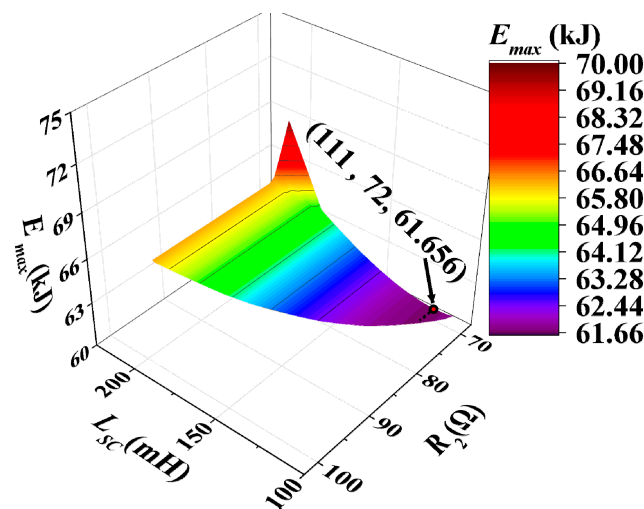


Figure 23. All feasible solutions of grid search in search space.

5.2.2. Optimization Results and Discussion

Based on two types of short-circuit calculation models and four workflows of optimization, eight parameter matching and optimization methods were obtained. Ten rounds of optimization were carried out by each of the eight methods, whose optimal results are compared with the global optimal solution of grid search in Table 7. Meanwhile the average performance parameters of each method are also listed in Table 7.

Table 7. The optimization results of different methods.

Method	Optimization Workflow	Optimal Parameters Combination					Number of Possible Solutions	Number of Iterations	Average Time (s)
		R_1 (Ω)	L_{SC} (mH)	R_2 (Ω)	E_{max} (kJ)	U_{S1max} (kV)			
Grid search	/	9	111	72	61.65590843	75.888	5539	5539	23,239
Hybird + GA	Workflow 1	9	111	72–75	61.65590843	75.8–79.1	799,526	71	9310
	Workflow 2	9	111	72	61.65590843	75.888	5539	54	7934
Hybird + PSO	Workflow 1	9	111	72–75	61.65590843	75.8–79.1	795,526	114	7577
	Workflow 2	9	111	72	61.65590843	75.888	5539	56	3748
Single + GA	Workflow 1	9	113	72–76	62.05086515	75.5–79.7	795,526	70	152
	Workflow 2	9	113	72	62.05086515	75.454	5539	55	105
Single + PSO	Workflow 1	9	113	72–76	62.05086515	75.5–79.7	795,526	109	121
	Workflow 2	9	113	72	62.05086515	75.454	5539	66	62

In Figure 24, with short-circuit calculation model and workflow unchanged, the convergence of PSO is slightly better than that of GA. Through horizontal comparisons with Workflow 1 in Figure 24a,c, it indicates that Workflow 2 had better convergence in Figure 24b,d. In addition, the convergence of the single short-circuit calculation models in Figure 24c,d are better than those of hybrid models in Figure 24a,b. Therefore, the combination of single model, PSO and Workflow 2 has the best convergence among the eight combinations of methods.

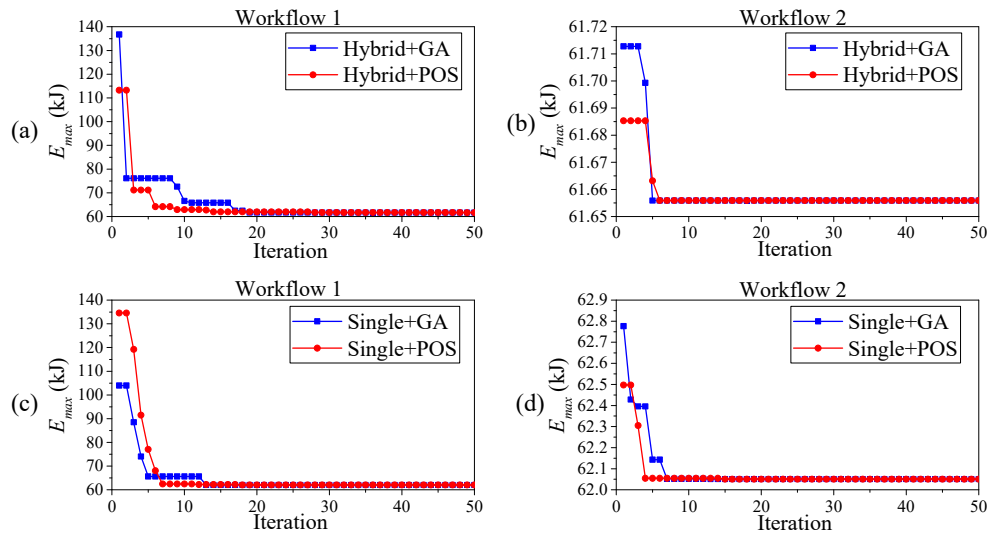


Figure 24. Convergence comparison of different methods: (a) Hybrid model + GA/PSO + Workflow 1; (b) Hybrid model + GA/PSO + Workflow 2; (c) Single model + GA/PSO + Workflow 1; (d) Single model + GA/PSO + Workflow 2.

According to Table 7, the number of possible solutions of each method in space and average running time of each method are respectively shown in Figure 25a,b. Grid search is the exhaustive method, obtaining global optimal solution by calculating every possible solution in space. In other words, it sacrifices solving time for solving accuracy. Therefore, it is the least efficient in searching among the several methods. In the hybrid model and the single model, the optimization algorithm of GA and PSO can more efficiently explore space to search global optimum solution, saving an amount of time in the face of a wider solution space. Compared with GA, PSO is simpler without the process of crossover and mutation and had a faster average solving speed. Compared with the hybrid model, because of simple structure, the single model could significantly shorten optimization time by an order of magnitude. In addition, by using parameter rules in the H-SFCL, possible solutions in space were effectively reduced. Therefore, Workflow 2 consumed less optimization time than Workflow 1. As such, the combination of the single model, PSO and Workflow 2 had the best optimization efficiency.

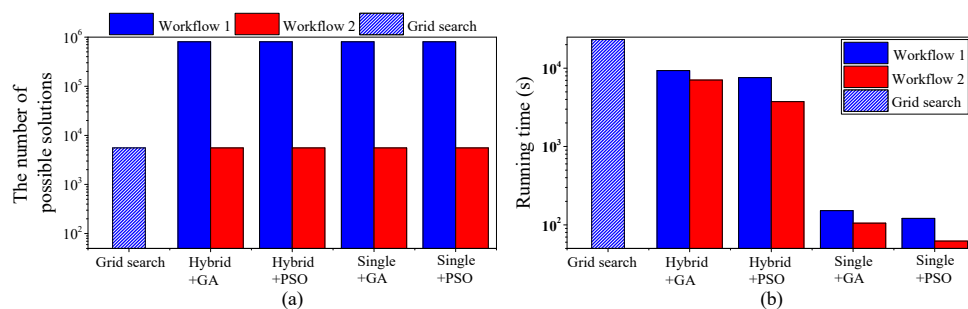


Figure 25. Optimization efficiency between different methods. (a) The number of possible solutions; (b) average running time of parameter matching and optimization methods.

Figure 26 reflects the ten rounds of optimization results for each method. The results of R_1 in eight optimization methods are consistent with the global optimal solution in Figure 26b. According to Section 4.2.1, the hybrid model had high calculation accuracy, while there was a certain error between the single model and full system model. Therefore, the single model introduced a fixed error for optimization results in Figure 26a,c. In the single model, compared with global optimal solution, the optimization results of E_{max} and L_{SC} had 0.64% and 1.8% errors, respectively. However, due to the high accuracy of the hybrid model, the optimization results of E_{max} , R_1 and L_{SC} in the hybrid model were consistent with global optimal solution.

Figure 26d shows that the optimization results of R_2 in Workflow 1 are unstable. The reason is that there are multiple solutions satisfying the minimum value of E_{max} . The feasible solutions of R_2 in the hybrid model are from 72Ω to 75Ω , while the feasible solutions of R_2 in single model are from 72Ω to 76Ω . Therefore, the optimization results of R_2 were random and unstable in Workflow 1. However, the links of results sorting and screening in Workflow 2 could effectively avoid this problem to select optimal parameters and increase the stability of optimization results. Therefore, the combination of the hybrid model, GA/PSO and Workflow 2 had the best optimization accuracy.

Based on the comparative analysis of the above different methods, the evaluations of their corresponding characteristics are listed in Table 8.

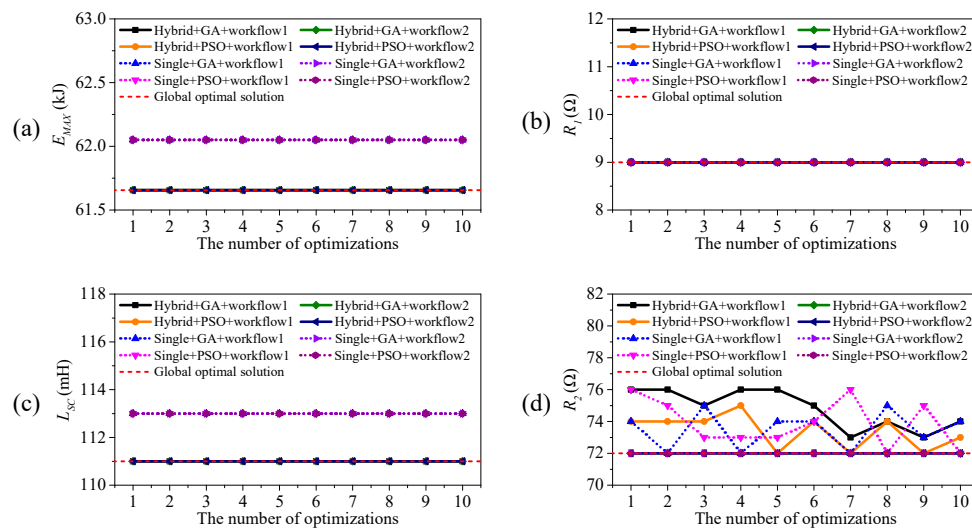


Figure 26. Ten rounds of optimization results for each method. (a) The optimization results of E_{max} ; (b) the optimization results of R_1 ; (c) the optimization results of L_{SC} ; (d) the optimization results of R_2 .

Table 8. The characteristics’ evaluation of parameter matching and optimization methods.

Method	Accuracy	Average Time Consuming	Search Range	Convergence Rate	Stability of Results
Grid search	★★★★★	★☆☆☆☆	★★★★☆	/	★★★★★
Hybird + GA	Workflow 1	★★★★☆	★★★★★	★★★★☆	★★☆☆☆
	Workflow 2	★★★★★	★★★★☆	★★★★☆	★★★★★
Hybird + PSO	Workflow 1	★★★★☆	★★★★★	★★★★☆	★★☆☆☆
	Workflow 2	★★★★★	★★★★☆	★★★★☆	★★★★★
Single + GA	Workflow 1	★★★★☆	★★★★★	★★★★☆	★★☆☆☆
	Workflow 2	★★★★☆	★★★★★	★★★★☆	★★★★☆
Single + PSO	Workflow 1	★★★★☆	★★★★★	★★★★☆	★★☆☆☆
	Workflow 2	★★★★☆	★★★★★	★★★★☆	★★★★★

Excellent ★★★★★, Very Good ★★★★☆, Good ★★★☆☆, Fair ★★☆☆☆, Poor ★☆☆☆☆.

According to the method combinations of hybrid model, GA/PSO and Workflow 2, the global optimal parameters combinations the of H-SFCL are $(R_1, L_{SC}, R_2) = (9, 111, 72)$, which are brought into the VSC-based DC system simulation model for validation. Simulation results included DC line current, equivalent current limiting impedance of the H-SFCL, the current of L_{SC} branch and the overvoltage of S_1 , as shown in Figure 27. This clearly indicates that optimization parameters can meet target requirements. Therefore, the above methods are effective and feasible.

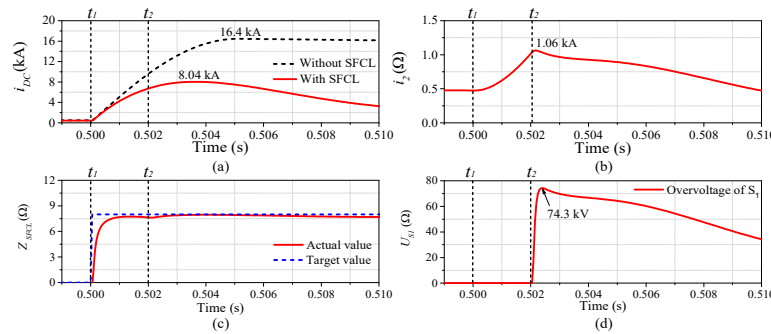


Figure 27. Simulation verification of optimization results. (a) DC line current; (b) the current of superconducting coil; (c) current limiting impedance; (d) the overvoltage of S_1 .

5.3. Comparative Analysis between Unoptimized and Optimized Parameters of H-SFCL

In order to verify the optimizing function of parameter matching and optimization methods, a group of non-optimal parameters with the similar current limiting rate were selected to compare with the optimized parameters of the H-SFCL in simulation. According to Table 3, current limiting rate mainly depends on R_1 . Therefore, a group of arbitrary non-optimal parameters were selected as follows: $R_1 = 9 \Omega$, $R_2 = 20 \Omega$, $L_{SC} = 140 \text{ mH}$. Its current limiting rate was also about 50%. The comparative analysis was carried out from three aspects: VSC-based DC system, DCCB and H-SFCL.

5.3.1. Comparative Analysis in VSC-Based DC System

According to Figure 28, DC fault occurs at 0.5 s. Unoptimized H-SFCL had the same current limiting rate as the optimized H-SFCL, so there was no significant difference between their effects on a VSC-based DC system from 0.5 s to 0.505 s. However, because of the optimized H-SFCL, the minimum DC side voltage of the system was higher after 0.510 s, as shown in Figure 28a. Meanwhile, fault current was slightly lower in the DC line and converter, as shown in Figure 28b,c. In other words, though the current limiting rates of two H-SFCLs both matched the requirements of the system, the optimized H-SFCL shows slightly better performance of voltage compensation and current limiting than those of the unoptimized H-SFCL in continuous fault.

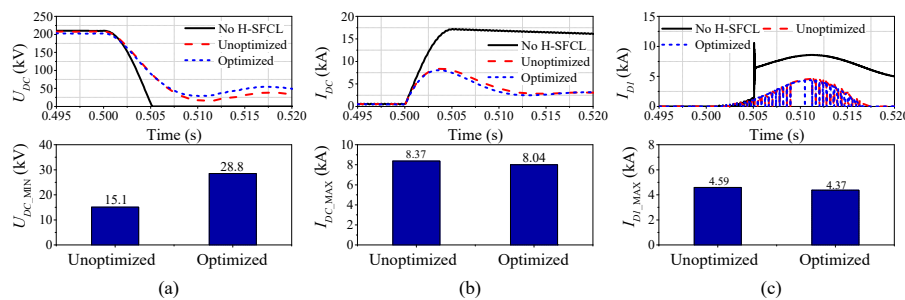


Figure 28. Comparison simulation results for VSC-based DC system. (a) DC side voltage; (b) DC line current; (c) the current of freewheel diode.

5.3.2. Comparative Analysis in DCCB

Figure 29a–c indicate that the H-SFCL can effectively suppress voltage stress, breaking current and energy absorbed of the CM-DCCB and H-DCCB. However, the maximum voltage stress and breaking current of the two types of DCCBs mainly depended on current limiting rate. Therefore, if current limiting rate remains unchanged, they will not be obviously affected by parameter optimization of the H-SFCL, as shown in Figure 29a,b,d,e. But it is worth noting that the optimized H-SFCL can make the CM-DCCB and H-DCCB absorb less energy with the same current limiting rate. The reason is that the optimized H-SFCL has higher steady current limiting impedance in Figure 29d, which can absorb more energy from the system released to alleviate energy shock on the DCCB.

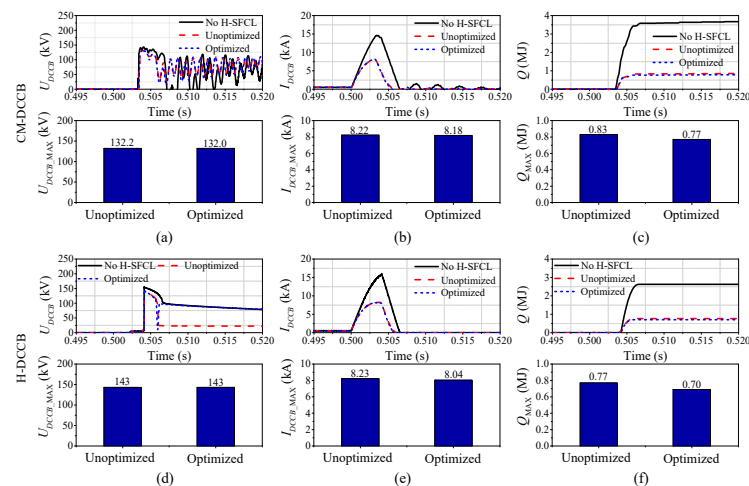


Figure 29. Comparison simulation results for DCCB. (a) The voltage of CM-DCCB; (b) the breaking current of CM-DCCB; (c) the absorbed energy of CM-DCCB; (d) the voltage of H-DCCB; (e) the breaking current of H-DCCB; (f) the absorbed energy of H-DCCB.

5.3.3. Comparative Analysis in H-SFCL

Figure 30a shows that the overcurrent of the superconducting coil in the optimized H-SFCL was much lower than the unoptimized H-SFCL, with 44% reduction. It clearly indicates the effect of overcurrent on the superconducting coil was significantly weakened by parameter optimization. In Figure 30b, though superconducting coils were subjected to the same maximum voltage stress in the unoptimized and optimized H-SFCLs, a shorter duration of overvoltage is seen in the optimized H-SFCL. In Figure 30c, during current limiting process, the maximum magnetic energy in the optimized H-SFCL is 62 kJ, which was only about 25% of that in the unoptimized H-SFCL. On the premise that the current limiting rate was not affected, the fluctuation of magnetic energy can be effectively suppressed by parameter optimization in the H-SFCL, avoiding a superconducting coil with excessive transient loss and cost. In addition, the optimized H-SFCL presents a more stable current limiting impedance curve than the unoptimized H-SFCL in Figure 30d. However, the optimization cannot improve performance parameters of all components. Figure 30e,f suggest that a S_1 with larger breaking capacity is needed in the optimized H-SFCL, but the change of S_1 caused by optimization still meets the target value of constraint conditions.

5.3.4. Summary

According to the above simulation research, corresponding results are listed in Table 9. On the premise of the same current limiting rate, the optimized H-SFCL shows a slightly better effect on the system and DCCB than the unoptimized H-SFCL, but these differences are not significant. For the same kind of H-SFCL, the influence of the H-SFCL on external systems and devices is mainly affected

by its current limiting rate. Therefore, when the current limiting rate of the H-SFCL reaches the target value, the H-SFCL can meet the current limiting requirements of the system and DCCB.

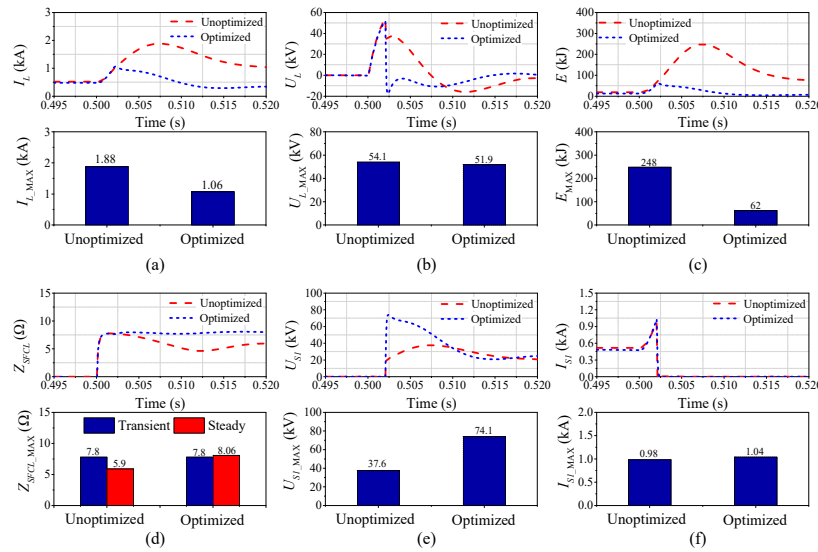


Figure 30. Comparison simulation results for H-SFCL. (a) The overcurrent of superconducting coil; (b) the overvoltage of superconducting coil; (c) the magnetic energy of superconducting coil; (d) equivalent current limiting impedance; (e) the overvoltage of S_1 ; (f) the breaking current of S_1 .

Table 9. The effects of comparison between unoptimized and optimized H-SFCL.

Parameters		Unoptimized H-SFCL	Optimized H-SFCL	Improvement	Influence Degree	
Optimization variable	R_1	9 Ω	9 Ω	0%	/	
	L_{SC}	140 mH	111 mH	20.71%↓		
	R_2	20 Ω	72 Ω	250%↑		
VSC-based DC system	Minimum U_{DC}	15.1 kV	28.8 kV	90.73%↑	★★☆☆☆	
	Maximum I_{DC}	8.37 kA	8.04 kA	3.9%↓		
	Maximum I_{D1}	4.59 kA	4.37 kA	4.79%↓		
DCCB	M-DCCB	Maximum U_{DCCB}	132.2 kV	130.0 kV	1.66%↓	★☆☆☆☆
		Maximum I_{DCCB}	8.22 kA	8.18 kA	0.49%↓	
		Absorbed Energy	0.83 kJ	0.77 kJ	7.22%↓	
	H-DCCB	Maximum U_{DCCB}	143 kV	143 kV	0%	
		Maximum I_{DCCB}	8.23 kA	8.04 kA	2.31%↓	
		Absorbed Energy	0.77 kJ	0.70 kJ	9.09%↓	
H-SFCL	Superconducting coil	Maximum I_L	1.88 kA	1.06 kA	43.62%↓	★★★★★
		Maximum U_L	54.1 kV	51.9 kV	4.07%↓	
		Duration of Overvoltage	7 ms	4 ms	42.86%↓	
		Maximum E	248 kJ	62 kJ	75%↓	
	Z_{SFCL}	Transient Z_{SFCL}	7.8 Ω	7.8 Ω	0%	
		Steady Z_{SFCL}	5.9 Ω	8.06 Ω	36.61%↑	
	S_1	Maximum U_{S1}	37.6 kV	74.1 kV	97.07%↑	
Maximum I_{S1}		0.98 kA	1.04 kA	6.12%↑		

Excellent ★★★★★, Very Good ★★★★☆, Good ★★★☆☆, Fair ★★☆☆☆, Poor ★☆☆☆☆.

However, on the premise of meeting current limiting requirements and other operational indicators, the parameter matching and optimization method of the H-SFCL can select better matching parameters of R_1 , L_{SC} and R_2 . Taking the maximum magnetic energy of the superconducting coil as an optimization target can significantly reduce multiple performance indicators of the superconducting coil, such as maximum I_L , overvoltage U_L , inductance value and transient magnetic energy. This improvement can

contribute to reduce the loss and cost of the H-SFCL with more stable performance. Therefore, the optimization function of this method has been well verified.

6. Conclusions

The parameter matching in the SFCL not only has an important impact on suppressing short-circuit fault current and maintaining the stability of a VSC-based system, but also affects the performance advantages, reliability and cost of the SFCL itself. Therefore, for the H-SFCL developed by our laboratory, eight method combinations of parameter matching and optimization are put forward based on two short-circuit calculation models, two algorithms and two workflows, whose effectiveness of optimization are well verified in system simulation.

Through simulation and comparative analysis, the characteristics of these methods are clearly elucidated as follows:

- (1) In the aspect of short-circuit calculation, the hybrid model has high solution accuracy and wider range of accuracy, but calculation speed is relatively slow. The single model is simple with outstanding solution speed, but its calculation accuracy is general.
- (2) In the aspect of algorithms, PSO has simpler structure, slightly better convergence and faster optimization speed than GA. However, GA is more mature and is an easier operation with the optimization tool in MATLAB. Compared with grid search (exhaustion method), GA and PSO both have more efficient search ability for an optimal solution in complex space, significantly reducing computational load and improving optimization efficiency.
- (3) In the aspect of optimization workflows, Workflow 1 is simple and easier to implement, but its results are not stable. Workflow 2 is the improvement of Workflow 1, which can obtain global optimal parameters of the H-SFCL faster and more stably.

Therefore, “single model + PSO + Workflow 2” is the optimal method combination with the fastest optimization speed, while “hybrid model + GA or PSO + Workflow 2” is the optimal method combination with the highest optimization accuracy. For contradictions among the effects of multiple parameters, these methods can select a good parameter matching scheme and maximize the performance advantages of the SFCL to meet the current limiting requirements of VSC-based systems. Meanwhile, optimizing the magnetic energy of the superconducting coil can significantly reduce the peak value of overvoltage, the duration of overvoltage, overcurrent and magnetic energy, thereby effectively reducing the cost and operation conditions of the H-SFCL.

It is worth noting that these methods are not limited to the parameter matching and optimization of the H-SFCL. By adjusting constraints and optimizing objectives, they can balance the relationships among multiple parameters and provide good references for the optimization issues of other current limiters or equipment applied in power systems.

Author Contributions: Conceptualization, S.L.; Data curation, J.S.; Formal analysis, S.L. and X.T.; Investigation, X.T., Z.L.; Methodology, S.L. and L.R.; Software, S.L. and Y.X.; Supervision, Y.T.; Validation, S.L., X.T., Z.L. and J.S.; Writing—original draft, S.L.; Writing—review & editing, L.R.

Funding: This research was funded by the Project of the National Natural Science Foundation of China under grant number 51677080.

Conflicts of Interest: The authors declare no conflict of interest.

Nomenclature

VSC	Voltage Source Converter	CB	Circuit Breaker
MMC	Modular Multilevel Converter	SFCL	Superconducting Fault Current Limiter
HVDC	High Voltage Direct Current	RCB	Residual Circuit Breaker
HTS	High temperature superconducting	UFD	Ultra Fast Disconnecter
DC	Direct Current	MB	Main Breaker
AC	Alternating Current	LCS	Load Commutation Switch

MTDC	Multi-terminal Direct Current	MOV	Metal Oxide Varistor
H-	Hybrid Type	GA	Genetic Algorithm
CM-	Coupling Mechanical	PSO	Particle Swarm Optimization
IGBT	Insulated Gate Bipolar Transistor	SCR	silicon controlled rectifier

Symbols

Δt	Breaking delay time of S_1 (s)	i_1	Current of R_1 branch in H-SFCL (A)
t_{det}	Fault protection time (s)	i_L	Current of superconducting coil (A)
t_{cod}	Protection coordination time (s)	I_{D1}	Current of freewheel diode (A)
t_{com}	Communication time (s)	I_{DC}	DC line current (A)
i_{DC}	DC line current (A)	I_{S1}	Current of S_1 (A)
t_1	The time of fault occurrence (s)	I_C	Critical current of L_{SC} (A)
t_2	S_1 switch breaking time (s)	U_L	Overvoltage of L_{SC} (V)
U_{DC}	DC side voltage (V)	U_{S1}	Overvoltage of S_1 (V)
U_c	DC-link capacitor voltage (V)	E	Magnetic energy of L_{SC} (J)
R	Line resistance (Ω)	E_{max}	Maximum magnetic energy (J)
R_L	Equivalent load on DC side (Ω)	Z_{SFCL}	Current limiting impedance (Ω)
L	Line inductance (H)	I_p	Peak value of fault current (A)
C	DC-link capacitance (F)	I_{Lmax}	Maximum current value of L_{SC} (A)
R_1	Current limiting resistance (Ω)	I_{rated}	Rated DC-line current (A)
R_2	Current limiting resistance (Ω)	U_{rated}	Rated voltage of S_1 (V)
L_{SC}	Inductance of HTS coil (H)	K	Fault current limiting rate

References

1. Chehardeh, M.I.; Lesani, H.; Zadeh, M.K. An optimal control strategy to alleviate sub-synchronous resonance in VSC-HVDC systems. In Proceedings of the 2009 2nd International Conference on Power Electronics and Intelligent Transportation System (PEITS), Shenzhen, China, 19–20 December 2009; pp. 250–255.
2. Huang, Y.; Yuan, X.; Hu, J. DC-Bus Voltage Control Stability Affected by AC-Bus Voltage Control in VSCs Connected to Weak AC Grids. *IEEE J. Emerg. Sel. Top. Power Electron.* **2016**, *4*, 445–458. [[CrossRef](#)]
3. Zheng, C.; Zhou, X.; Li, R. Dynamic Modeling and Transient Simulation for VSC based HVDC in Multi-Machine System. In Proceedings of the 2006 International Conference on Power System Technology, Chongqing, China, 22–26 October 2006; pp. 1–7.
4. Xu, Z.; Li, R.; Hu, B. Direct power control based on renewable energy access for VSC-HVDC system. In Proceedings of the IEEE 8th International Power Electronics and Motion Control Conference, Hefei, China, 22–26 May 2016; pp. 2319–2324.
5. DirkVan, H.; Ghandhari, M. Multi-terminal VSC HVDC for the European supergrid: Obstacles. *Renew. Sustain. Energy Rev.* **2010**, *14*, 3156–3163.
6. Flourentzou, N.; Agelidis, V.G.; Demetriades, G.D. VSC-Based HVDC Power Transmission Systems: An Overview. *IEEE Trans. Power Electron.* **2009**, *24*, 592–602. [[CrossRef](#)]
7. Dorn, J.; Gambach, H.; Retzmann, D. HVDC transmission technology for sustainable power supply. In Proceedings of the International Multi-Conference on Systems, Signals & Devices, Chemnitz, Germany, 20–23 March 2012; pp. 1–6.
8. Barnes, M.; Beddard, A. Voltage Source Converter HVDC Links-The State of the Art and Issues Going Forward. *Energy Procedia* **2012**, *24*, 108–122. [[CrossRef](#)]
9. Fu, J.; Yuan, Z.; Wang, Y. Control strategy of system coordination in Nanao multi-terminal VSC-HVDC project for wind integration. In Proceedings of the IEEE PES General Meeting, National Harbor, MD, USA, 27–31 July 2014; pp. 1–5.
10. Yang, J.; Yang, Y.; He, Z. System design of MMC VSC-HVDC demonstration project for windfarm connection. In Proceedings of the 10th IET International Conference on AC and DC Power Transmission (ACDC 2012), Birmingham, UK, 4–5 December 2012; pp. 1–6.

11. Jovcic, D.; Van Hertem, D.; Linden, K. Feasibility of DC transmission networks. In Proceedings of the 2011 2nd IEEE PES International Conference and Exhibition on Innovative Smart Grid Technologies, Manchester, UK, 5–7 December 2011; pp. 1–8.
12. Monadi, M.; Koch-Ciobotaru, C.; Luna, A. Multi-terminal medium voltage DC grids fault location and isolation. *IET Gener. Transm. Dis.* **2016**, *10*, 3517–3528. [[CrossRef](#)]
13. Wang, Y.; Yuan, Z.; Wen, W. Generalised protection strategy for HB-MMC-MTDC systems with RL-FCL under DC faults. *IET Gener. Transm. Dis.* **2018**, *12*, 1231–1239. [[CrossRef](#)]
14. Yang, J.; Fletcher, J.E.; O'Reilly, J. Short-Circuit and Ground Fault Analyses and Location in VSC-Based DC Network Cables. *IEEE Trans. Ind. Electron.* **2012**, *59*, 3827–3837. [[CrossRef](#)]
15. Tang, L.; Ooi, B.T. Locating and Isolating DC Faults in Multi-Terminal DC Systems. *IEEE Trans. Power Del.* **2007**, *22*, 1877–1884. [[CrossRef](#)]
16. Li, Y.; Shi, X.; Wang, F. Dc fault protection of multi-terminal VSC-HVDC system with hybrid dc circuit breaker. In Proceedings of the 2016 IEEE Energy Conversion Congress and Exposition (ECCE), Milwaukee, WI, USA, 18–22 September 2016; pp. 1–8.
17. Gomis-ellmunt, O.; Liang, J.; Ekanayake, J. Topologies of multiterminal HVDC-VSC transmission for large offshore wind farms. *Electr. Pow. Syst. Res.* **2011**, *81*, 271–284. [[CrossRef](#)]
18. Chen, L.; Chen, H.; Shu, Z.; Zhang, G. Comparison of Inductive and Resistive SFCL to Robustness Improvement of a VSC-HVDC System with Wind Plants Against DC Fault. *IEEE Trans. Appl. Supercond.* **2016**, *26*, 5603508. [[CrossRef](#)]
19. Yang, Q.; Blond, S.L.; Liang, F. Design and Application of Superconducting Fault Current Limiter in a Multiterminal HVDC System. *IEEE Trans. Appl. Supercond.* **2017**, *27*, 3800805. [[CrossRef](#)]
20. Khan, U.A.; Lee, J.G.; Amir, F. A Novel Model of HVDC Hybrid-Type Superconducting Circuit Breaker and Its Performance Analysis for Limiting and Breaking DC Fault Currents. *IEEE Trans. Appl. Supercond.* **2015**, *25*, 5603009.
21. Yang, K.; Yang, Y.; Junaid, M. Direct-Current Vacuum Circuit Breaker with Superconducting Fault-Current Limiter. *IEEE Trans. Appl. Supercond.* **2018**, *28*, 5600108. [[CrossRef](#)]
22. Lee, J.G.; Khan, U.A. Impact of SFCL on the Four Types of HVDC CBs by Simulation. *IEEE Trans. Appl. Supercond.* **2016**, *26*, 5602606. [[CrossRef](#)]
23. Li, B.; Wang, C.; Wei, Z. Technical Requirements of the DC Superconducting Fault Current Limiter. *IEEE Trans. Appl. Supercond.* **2018**, *28*, 5602805. [[CrossRef](#)]
24. Li, B.; He, J. Studies on the Application of R-SFCL in the VSC-Based DC Distribution System. *IEEE Trans. Appl. Supercond.* **2016**, *26*, 5601005. [[CrossRef](#)]
25. Chen, L.; He, H.; Li, G. Study of Resistive-Type Superconducting Fault Current Limiters for a Hybrid High Voltage Direct Current System. *Materials* **2018**, *12*, 26. [[CrossRef](#)]
26. Leon Garcia, W.R.; Tixador, P.; Raison, B. Technical and Economic Analysis of the R-Type SFCL for HVDC Grids Protection. *IEEE Trans. Appl. Supercond.* **2017**, *27*, 5602009. [[CrossRef](#)]
27. Xiao, L.; Dai, S.; Lin, L. HTS Power Technology for Future DC Power Grid. *IEEE Trans. Appl. Supercond.* **2013**, *23*, 5401506. [[CrossRef](#)]
28. Fisher, L.M.; Alferov, D.F.; Akhmetgareev, M.R. A superconducting direct-current limiter with a power of up to 8 MVA. *Phys. Atom. Nucl.* **2017**, *79*, 1577–1584. [[CrossRef](#)]
29. Pascal, P.T.; Badel, A.; Auram, G. Superconducting Fault Current Limiter for Ship Grid Simulation and Demonstration. *IEEE Trans. Appl. Supercond.* **2017**, *27*, 5601705. [[CrossRef](#)]
30. Wang, C.; Li, B.; He, J. Design and Application of the SFCL in the Modular Multilevel Converter Based DC System. *IEEE Trans. Appl. Supercond.* **2017**, *27*, 3800504. [[CrossRef](#)]
31. Li, B.; Jing, F.; Li, B. Study of the Application of Active Saturated Iron-Core Superconductive Fault Current Limiters in the VSC-HVDC System. *IEEE Trans. Appl. Supercond.* **2018**, *28*, 5602906. [[CrossRef](#)]
32. Lee, H.Y.; Asif, M.; Park, K.H. Feasible Application Study of Several Types of Superconducting Fault Current Limiters in HVDC Grids. *IEEE Trans. Appl. Supercond.* **2018**, *28*, 5601205. [[CrossRef](#)]
33. Zhang, L.; Shi, J.; Wang, Z. Application of a Novel Superconducting Fault Current Limiter in a VSC-HVDC System. *IEEE Trans. Appl. Supercond.* **2017**, *27*, 5600706. [[CrossRef](#)]
34. Li, B.; Jiang, F.; Li, B.; Wen, W. Research on the Parameter Matching Between Active SI-SFCL and DC Circuit Breaker in DC systems. *IEEE Trans. Appl. Supercond.* **2019**, *29*, 5601605. [[CrossRef](#)]

35. Lee, H.Y.; Asif, M.; Park, K.H. Appropriate Protection Scheme for DC Grid Based on the Half Bridge Modular Multilevel Converter System. *Energies* **2019**, *12*, 1837. [[CrossRef](#)]
36. Khazali, A.; Kalantar, M. Optimal power flow considering fault current level constraints and fault current limiters. *Int. J. Elect. Power Energy Syst.* **2014**, *59*, 204–213. [[CrossRef](#)]
37. Didier, G.; Lévêque, J. Influence of fault type on the optimal location of superconducting fault current limiter in electrical power grid. *Int. J. Elect. Power Energy Syst.* **2014**, *56*, 279–285. [[CrossRef](#)]
38. Yu, P.; Venkatesh, B.; Yazdani, A. Optimal Location and Sizing of Fault Current Limiters in Mesh Networks Using Iterative Mixed Integer Nonlinear Programming. *IEEE Trans. Power Syst.* **2016**, *31*, 4776–4783. [[CrossRef](#)]
39. Zhang, X.; Ruiz, H.S.; Geng, J. Optimal location and minimum number of superconducting fault current limiters for the protection of power grids. *Int. J. Elect. Power Energy Syst.* **2017**, *87*, 136–143. [[CrossRef](#)]
40. Hamidi, M.E.; Chabanloo, R.M. Optimal Allocation of Distributed Generation with Optimal Sizing of Fault Current Limiter to Reduce the Impact on Distribution Networks Using NSGA-II. *IEEE Syst. J.* **2019**, *13*, 1714–1724. [[CrossRef](#)]
41. Chen, L.; Zhang, X.; Chen, H. Pareto optimal allocation of resistive-type fault current limiters in active distribution networks with inverter-interfaced and synchronous distributed generators. *Energy Sci. Eng.* **2019**. [[CrossRef](#)]
42. Wang, W.; Jazebi, S. Looping Radial Distribution Systems Using Superconducting Fault Current Limiters: Feasibility and Economic Analysis. *IEEE Trans. Power Syst.* **2018**, *33*, 2486–2495. [[CrossRef](#)]
43. Elmitwally, A.; Guoda, E.; Eladawy, S. Restoring recloser-fuse coordination by optimal fault current limiters planning in DG-integrated distribution systems. *Int. J. Elect. Power Energy Syst.* **2016**, *77*, 1–10. [[CrossRef](#)]
44. Liang, S.; Tang, Y.; Xia, Z. Study on the Current Limiting Performance of a Novel SFCL in DC Systems. *IEEE Trans. Appl. Supercond.* **2017**, *27*, 5601106. [[CrossRef](#)]
45. Liang, S.; Tang, Y.; Ren, L. Tests and Analysis of a Small-Scale Hybrid-Type DC SFCL Prototype. *IEEE Trans. Appl. Supercond.* **2018**, *27*, 5602106. [[CrossRef](#)]
46. Pei, X.; Cwikowski, O.; Vilchis-Rodriguez, D.S. A review of technologies for MVDC CBs. In Proceedings of the IECON 2016—42nd Annual Conference of the IEEE Industrial Electronics Society, Florence, Italy, 23–26 October 2016; pp. 3799–3805.
47. Qi, L.L.; Antoniazzi, A.; Raciti, L. Design of Solid-State Circuit Breaker-Based Protection for DC Shipboard Power Systems. *IEEE J. Emerg. Sel. Topics Power Electron.* **2017**, *5*, 260–268. [[CrossRef](#)]
48. Xue, S.M.; Liu, C. Line-to-Line Fault Analysis and Location in a VSC-Based Low-Voltage DC Distribution Network. *Energies* **2018**, *11*, 536. [[CrossRef](#)]
49. Callavik, M.; Blomberg, A.; Häfner, J. *The Hybrid HVDC Breaker An Innovation Breakthrough Enabling Reliable HVDC Grids*; ABB Grid Systems, Technical Paper; ABB: Zürich, Switzerland, 2012.
50. Xiao, L.; Sheng, C.; Lu, Q. Research on Short-Circuit Test and Simulation of CSG First Mechanical HVDC Circuit Breaker in VSC-HVDC. In Proceedings of the 2018 International Conference on Power System Technology (POWERCON), Guangzhou, China, 6–8 November 2018; pp. 2764–2769.
51. Zhang, Z.; Li, X.; Chen, M. Research and Development of 160kV Ultra-Fast Mechanical HVDC Circuit Breaker. *Power Syst. Technol.* **2018**, *42*, 2331–2338.
52. Yeap, Y.M.; Geddada, N.; Satpathi, K. Time and Frequency Domain Fault Detection in VSC Interfaced Experimental DC Test System. *IEEE Trans. Ind. Informat.* **2018**, *14*, 4353–4364. [[CrossRef](#)]
53. Park, D.K.; Bang, J.S.; Yang, S.E. Theoretical and Experimental Analysis of AC Loss Characteristic of Bifilar Pancake Coil with Coated Conductor. *IEEE Trans. Appl. Supercond.* **2008**, *18*, 1232–1235. [[CrossRef](#)]
54. Xu, Y.; Ren, L.; Tang, Y. A Study on the Design and Comparison of 1–100-MJ-Class SMES Magnet with Different Coil Configurations. *IEEE Trans. Appl. Supercond.* **2017**, *27*, 5700809. [[CrossRef](#)]
55. Bintha, S.; Sathya, S.S. A survey of Bio inspired optimization algorithms. *Int. J. Soft Comput. Eng.* **2012**, *2*, 137–151.
56. Michalewicz, Z. *Genetic Algorithms + Data Structures = Evolution Programs*; Springer: New York, NY, USA, 1999.
57. Haupt, R.L.; Haupt, S.E. *Practical Genetic Algorithms*; John Wiley & Sons: Hoboken, NJ, USA, 2004.
58. Teng, J.H.; Lu, C.N. Optimum fault current limiter placement with search space reduction technique. *IET Gener. Trans. Distrib.* **2010**, *4*, 485–494. [[CrossRef](#)]

59. Huang, J.; Hu, X.; Yang, F. Support vector machine with genetic algorithm for machinery fault diagnosis of high voltage circuit breaker. *Measurement* **2011**, *44*, 1018–1027. [[CrossRef](#)]
60. Ebrahim, M.A.; Elyan, T.; Wadie, F.; Abd-Allah, M.A. Optimal design of RC snubber circuit for mitigating transient overvoltage on VCB via hybrid FFT/Wavelet Genetic approach. *Electric Power Syst. Res.* **2017**, *143*, 451–461. [[CrossRef](#)]
61. Kennedy, J.; Eberhart, R. Particle swarm optimization. In Proceedings of the ICNN'95—International Conference on Neural Networks, Perth, WA, Australia, 27 November–1 December 1995; Volume 4, pp. 1942–1948.
62. Mehdinejad, M.; Mohammadi-Ivatloo, B. Solution of optimal reactive power dispatch of power systems using hybrid particle swarm optimization and imperialist competitive algorithms. *Int. J. Elect. Power Energy Syst.* **2016**, *83*, 104–116. [[CrossRef](#)]
63. Farahmand, H.; Rashidinejad, M.; Mousavi, A. Hybrid Mutation Particle Swarm Optimisation method for Available Transfer Capability enhancement. *Int. J. Elect. Power Energy Syst.* **2012**, *42*, 240–249. [[CrossRef](#)]
64. Kerdphol, T.; Fuji, K.; Mitani, Y. Optimization of a battery energy storage system using particle swarm optimization for stand-alone microgrids. *Int. J. Elect. Power Energy Syst.* **2016**, *81*, 32–39. [[CrossRef](#)]



© 2019 by the authors. Licensee MDPI, Basel, Switzerland. This article is an open access article distributed under the terms and conditions of the Creative Commons Attribution (CC BY) license (<http://creativecommons.org/licenses/by/4.0/>).